



1

1 **Anthropogenic activities significantly increase annual**  
2 **greenhouse gas (GHG) fluxes from temperate headwater**  
3 **streams in Germany**

4 **Authors:** Ricky Mwangada Mwanake<sup>1</sup>; Gretchen Maria Gettel<sup>2</sup>, Elizabeth Gachibu Wangari<sup>1</sup>,  
5 Clarissa Glaser<sup>5</sup>, Tobias Houska<sup>4</sup>, Lutz Breuer<sup>4,6</sup>, Klaus Butterbach-Bahl<sup>1,3</sup>, Ralf Kiese<sup>1</sup>

6

7 <sup>1</sup>Karlsruhe Institute of Technology, Institute for Meteorology and Climate Research, Atmospheric

8 Environmental Research (IMK-IFU), Kreuzeckbahnstrasse 19, Garmisch-Partenkirchen 82467, Germany

9 <sup>2</sup>IHE-Delft Institute for Water Education, Westvest 7 2611 AX Delft the Netherlands

10 <sup>3</sup>Pioneer Center Land-CRAFT, Department of Agroecology, University of Aarhus, Denmark

11 <sup>4</sup>Institute for Landscape Ecology and Resources Management (ILR), Research Centre for BioSystems, land use /  
12 land cover and Nutrition (iFZ), Justus Liebig University Giessen, Giessen, 35392, Germany

13 <sup>5</sup>Center for Applied Geoscience, University of Tübingen, Tübingen, Germany

14 <sup>6</sup>Centre for International Development and Environmental Research (ZEU), Justus Liebig University Giessen,  
15 Senckenbergstrasse 3, 35390 Giessen, Germany

16

17 *Correspondence to Ralf Kiese (ralf.kiese@kit.edu)*

18 **Abstract**

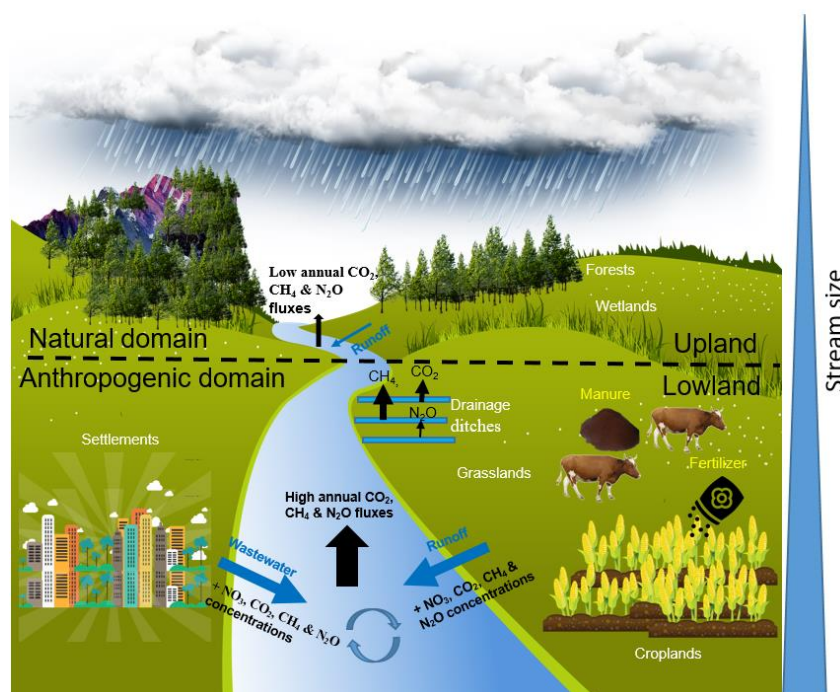
19 Anthropogenic activities increase the contributions of inland waters to global greenhouse gas (GHG;  
20 CO<sub>2</sub>, CH<sub>4</sub>, and N<sub>2</sub>O) budgets, yet the mechanisms driving these increases are still not well constrained. In this  
21 study, we quantified year-long GHG concentrations and fluxes, as well as water physico-chemical variables from  
22 23 streams, 3 ditches, and 2 wastewater inflow sites across five headwater catchments in Germany contrasted by  
23 land use. Using mixed-effects models, we determined the overall impact of land use and seasonality on the intra-  
24 annual variabilities of these parameters. We found that land use was more significant than seasonality in  
25 controlling the intra-annual variability of GHG concentrations and fluxes. Agricultural land use and wastewater  
26 inflows in settlement areas resulted in up to 10 times higher daily riverine CO<sub>2</sub>, CH<sub>4</sub>, and N<sub>2</sub>O emissions than  
27 forested areas, as substrate inputs by these sources appeared to favor *in situ* GHG production processes.  
28 Dissolved GHG inputs directly from agricultural runoff and waste-water inputs also contributed substantially to  
29 the annual emissions from these sites. Drainage ditches were hotspots for CO<sub>2</sub> and CH<sub>4</sub> fluxes due to high  
30 dissolved organic matter concentrations, which appeared to favor *in situ* production via respiration and  
31 methanogenesis. Overall, the annual emission from anthropogenic-influenced streams in CO<sub>2</sub>-equivalents was up  
32 to 20 times higher (~71 kg CO<sub>2</sub> m<sup>-2</sup> yr<sup>-1</sup>) than from natural streams (~3 kg CO<sub>2</sub> m<sup>-2</sup> yr<sup>-1</sup>). Future studies aiming to  
33 estimate the contribution of lotic ecosystems to GHG emissions should therefore focus on anthropogenically  
34 perturbed streams, as their GHG emission are much more variable in space and time.



2

35 **Graphical abstract**

36



37



## 38 1 Introduction

39 Streams and rivers cover only a small fraction of the earth's land surface (Allen et al., 2018), yet they  
40 are significant contributors to global greenhouse gases (CO<sub>2</sub>, CH<sub>4</sub>, and N<sub>2</sub>O), emitting approximately 7.6 (6.1–  
41 9.1) Pg-CO<sub>2</sub> equivalent into the atmosphere per year. (Li et al., 2021). Several biogeochemical process are  
42 responsible for GHG production and consumption within fluvial ecosystems. CO<sub>2</sub> production is attributed to  
43 respiration of organic matter (Battin et al., 2008). Production of CH<sub>4</sub> occurs through methanogenesis, with  
44 carbon dioxide and acetic acid as substrates under anaerobic conditions (Stanley et al., 2016). Consumption of  
45 methane is also possible through methanotrophy in oxygen rich stream waters, producing CO<sub>2</sub> in the process  
46 (Shelley et al., 2014). N<sub>2</sub>O is mainly a byproduct in nitrification (under aerobic conditions) or an intermediate  
47 product in denitrification (under anaerobic conditions), but it can also be reduced to N<sub>2</sub> in organic-rich and  
48 nitrate-poor ecosystems (Quick et al., 2019).

49 Anthropogenic practices such as fertilizer application and construction of drainage ditches to allow  
50 agricultural use of former wetlands alter the rates of these processes, thereby influencing in-stream GHG  
51 dynamics (Peacock et al., 2021; Wallin et al., 2020; Mwanake et al., 2019). Elevated inorganic nitrogen in  
52 streams within fertilized croplands has been shown to favor in situ N<sub>2</sub>O (e.g., Beaulieu et al., 2009), CO<sub>2</sub>  
53 production (e.g., Bodmer et al., 2016; Borges et al., 2018), and CH<sub>4</sub> production (e.g., Mwanake et al., 2022).  
54 While such trends in agricultural streams show similarities across different catchment locations, GHG emissions  
55 from streams in predominantly forested catchments with minor influences from croplands and wetlands show  
56 more diverse patterns. Some studies indicated that forest streams are hotspots for GHG fluxes (e.g., Wallin et al  
57 ., 2018; Audet et al., 2019; Herreid et al., 2021), while others found the opposite with much lower fluxes in  
58 forests as compare to other land uses (e.g., Bodmer et al., 2016; Mwanake et al., 2022). Drainage ditches, which  
59 are characterized by short water residence times, high organic loads, and highly variable O<sub>2</sub> levels, can  
60 simultaneously support both aerobic and anaerobic organic carbon mineralization, driving vigorous CH<sub>4</sub> and  
61 CO<sub>2</sub> production and subsequent fluxes. In a recent meta-analysis, ditches and canals accounted for up to 3% of  
62 the global anthropogenic CH<sub>4</sub> emissions (Peacock et al., 2021). Yet, studies on them are scarce, and thus the  
63 main factors making them hotspots of carbon fluxes are still not well-constrained.

64 In fluvial ecosystems located in settlement areas, inflows of wastewater effluents also act as important  
65 drivers of GHG fluxes, by indirectly influencing insitu substrate availability for GHG production and through  
66 direct inflows of dissolved GHGs (e.g., Marescaux et al., 2018; Zhang et al., 2021; Wang et al., 2022). For  
67 example, in a study of urban-impacted rivers in the Seine basin in France, Marescaux et al. (2018) found  
68 elevated CO<sub>2</sub>, CH<sub>4</sub>, and N<sub>2</sub>O concentrations and fluxes downstream of wastewater inflows, which  
69 disproportionately contributed higher basin-wide annual GHG fluxes. Similar findings were also found in urban-  
70 impacted rivers in China, where GHG emissions were up to 14 times higher than from other land uses (Zhang et  
71 al., 2021). Yet, studies on GHG emissions from urban-impacted fluvial ecosystems are still scarce, and therefore  
72 their contributions to riverine annual GHG budgets are not well constrained. Moreover, little is known about the  
73 interactive effects of land use and wastewater effluent inflows on riverine GHG fluxes, and whether land use is  
74 the overarching controlling factor.



4

75 Under temperate climatic conditions, pronounced seasonality regulates the availability of nutrients and  
76 to some extent the O<sub>2</sub> in lotic ecosystems, which are both key factors driving *instream* GHG production and gas  
77 exchange rates (Borges et al., 2018; Rocher-Ros et al., 2019; Herreid et al., 2021; Aho et al., 2022). Cold winter  
78 periods are generally characterized by low *instream* carbon and nitrogen processing, which results in nutrient  
79 accumulation (e.g., Herreid et al., 2021), while high *instream* C and N processing are characteristic of warm  
80 summer periods (e.g., Borges et al., 2018; Aho et al., 2021, 2022). Seasonality in precipitation regulates  
81 discharge, whereby heavy precipitation events or snowmelt during spring result in high discharge events. At the  
82 same time, dry summers and winter periods are often characterized by lower discharge (e.g., Aho et al., 2022).  
83 Discharge in turn determines the water residence times in streams, thereby influencing rates of carbon and  
84 nitrogen processing (e.g., Borges et al., 2018; Mwanake et al., 2022). High discharge events may also increase  
85 dissolved GHG supply from upstream terrestrial sources and *instream* GHG production depending on the  
86 surrounding land use. For example, studies have found that during high discharge periods, streams draining  
87 wetlands show peak CO<sub>2</sub> and CH<sub>4</sub> concentrations (e.g., Aho et al., 2019; Borges et al., 2019) and pronounced  
88 N<sub>2</sub>O concentrations are found in streams of cropland dominated catchments (e.g., Mwanake et al., 2022).

89 The aforementioned interactions between seasonality and land use indicate that temporally sporadic  
90 measurements of GHG concentrations and fluxes are limited in revealing intra-annual variations, which are  
91 necessary for better estimating annual emissions. Yet, only a handful of studies in temperate streams have  
92 assessed the seasonal dynamics of GHG fluxes at sampling points with contrasting land uses (e.g., Marescaux et  
93 al., 2018; Borges et al., 2018; Herreid et al., 2021; Galantini et al., 2021). As climate change drives more  
94 extreme discharge conditions, and as agricultural intensification and settlement areas continue to increase  
95 (Winkler et al., 2021), studies that cover a wide array of land uses, discharge, and temperature conditions are  
96 needed to constrain better the effects of land use in controlling intra-annual GHG flux variabilities and to unravel  
97 synergistic or antagonistic relationships amongst them.

98 The main objective of this study was to assess the seasonality-land use relationships of water physico-  
99 chemical variables and GHG concentration and fluxes by comparing temperate lotic ecosystems of forests and  
100 wetlands with those from more human-influenced agricultural and settlement catchments. To do so, we  
101 conducted at least tri-weekly measurements covering a full year of observations and mainly focused on  
102 headwater streams (stream orders 1–6), which are known hotspots of fluvial emissions, but remain currently  
103 underrepresented in global GHG datasets (Drake et al., 2018; Li et al., 2021). We hypothesize that catchment  
104 land use is the most important control for stream GHG concentration and fluxes, with higher seasonal variability  
105 in human-influenced ecosystems than in natural ones. Moreover, we hypothesized that drainage ditches and  
106 headwater streams with wastewater inflow within agricultural and settlement areas are hotspots for GHG  
107 emissions, driven by direct dissolved GHG inputs or substrate inputs that favor *in situ* GHG production.

## 108 2 Materials and methods

### 109 2.1 Study areas and sampling design

110 Five headwater catchments in central (Schwingbach), southeast (Loisach), and southwest (Ammer,  
111 Goldersbach, and Steinlach) Germany were investigated in this study. The catchments covered a wide range of



5

112 fluvial ecosystems with different stream orders and land use characteristics (Table 1; Fig. 1). The catchment  
113 boundaries for each site were determined based on the most downstream sampling location within each  
114 catchment (Fig. 1). Elevation of the Schwingbach catchment (54 km<sup>2</sup>), located in the central-German state of  
115 Hessen, ranges from 176–480 m above sea level (a.s.l). The catchment has a mixed land use of ~41 % mixed  
116 forests, 46% croplands, 8 % settlement areas, and 5 % pasturelands (Wangari et al., 2022) (Fig. 1A). The climate  
117 is warm and temperate (Cfb, Köppen climate classification), with an annual rainfall of 742 mm (monthly mean  
118 min: 51 mm, monthly mean max: 72 mm) (1999–2019) and a mean annual temperature of 9.8 °C (monthly mean  
119 min: 1.3 °C, monthly mean max: 18.8 °C) (1991–2021) (Climate-data.org, [https://en.climate-  
120 data.org/europe/germany/hesse/giessen-151/](https://en.climate-data.org/europe/germany/hesse/giessen-151/)).

121 The Upper Loisach catchment (467 km<sup>2</sup>, outlet Eschenlohe town) is located in the mountainous region  
122 of the Bavarian Alps, Germany. The catchment is characterized by a pronounced relief and steep slopes, with  
123 elevations ranging from 616–2,963 m a.s.l. Land use in the catchment comprises coniferous and deciduous  
124 forests interspersed with natural grasslands and rocky surfaces on the mountain slopes (78%). At the valley  
125 bottom, the land use is mainly settlement areas (9%), managed grasslands (8%), and wetlands (5%) (Fig. 1B).  
126 The climate is cold and temperate (Dfb, Köppen climate classification), with annual precipitation of 1,693 mm  
127 (monthly mean min: 87 mm, monthly mean max: 207 mm) (1999–2019) and mean annual temperature of 3.8 °C  
128 (monthly mean min: -6.6 °C, monthly mean max: 13.1 °C) (1991–2021) (Climate-data.org, [https://en.climate-  
129 data.org/europe/germany/free-state-of-bavaria/garmisch-partenkirchen-8762/](https://en.climate-data.org/europe/germany/free-state-of-bavaria/garmisch-partenkirchen-8762/)).

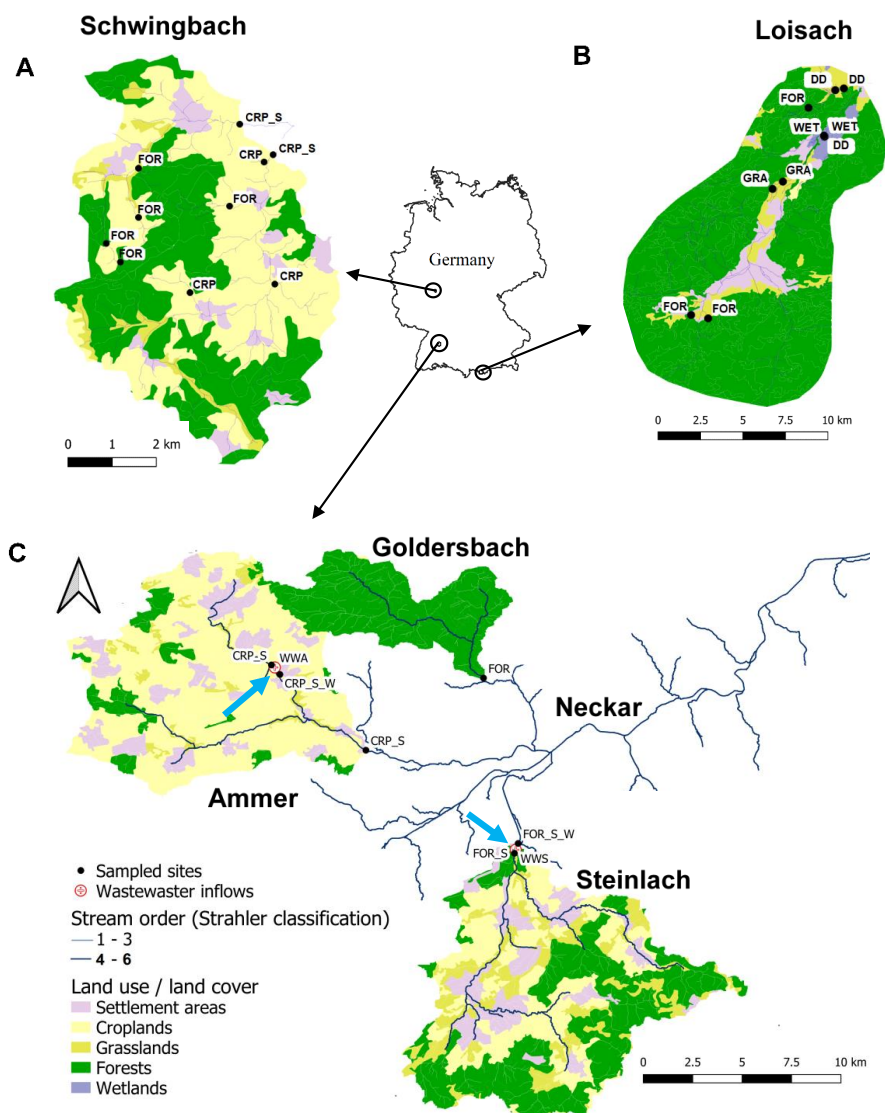
130 The other three catchments are sub-catchments of the Neckar river (Fig. 1C). The Goldersbach (116  
131 km<sup>2</sup>), a tributary of the main Ammer stream, is a forested catchment (95%), with elevations ranging from 366–  
132 583 m a.s.l. The Steinlach catchment (513 km<sup>2</sup>) is also dominated by forests (74%), with agricultural lands  
133 (croplands and grasslands) and settlement areas occupying 21% and 5% of the landscape, respectively. The  
134 elevation range of the hilly area is 321–878 m a.s.l (Fig. 1C). The Ammer catchment (304 km<sup>2</sup>, outlet  
135 Pfäffingen) is dominated by agricultural lands (80%), with 11% forests and 9% settlement areas (Fig. 1C). It has  
136 moderate slopes with an elevation ranging from 319–610 m a.s.l. The Ammer stream is a gaining stream fed by  
137 an extensive groundwater karst system and has significant discharge levels even during the driest periods of the  
138 year (Glaser et al., 2020). The climate is warm and temperate (Cfb, Köppen climate classification), with a mean  
139 annual rainfall of 923 mm (monthly mean min: 63 mm, monthly mean max: 98 mm) (1999–2019) and a mean  
140 annual temperature of 9.3 °C (monthly mean min: 0.2 °C, monthly mean max: 18.6 °C) (1991–2021) (Climate-  
141 data.org, [https://en.climate-  
142 data.org/europe/germany/baden-wuerttemberg/tuebingen-22712/](https://en.climate-data.org/europe/germany/baden-wuerttemberg/tuebingen-22712/)).

142 Across the five catchments, a total of 28 sites at headwater streams (N=23, orders 1–6, defined after  
143 Strahler, 1952), drainage ditches (N=3) and waste water outflows (N=2, Text A1) were sampled every 2–3 weeks  
144 for an entire year (Table 1, Fig. 1). The Schwingbach and Loisach catchments were sampled from June 2020 to  
145 June 2021 while the Goldersbach, Ammer, and Steinlach catchments, were sampled from April 2021 to April  
146 2022.

147



6



148

149

150 Fig. 1: Land cover maps of the (A) Schwingbach, (B) Loisach, and (C) Neckar sub-catchments (Goldersbach,  
 151 Ammer, and Steinlach) derived from the Corine Land Cover 2018 inventory with a 25 ha spatial resolution  
 152 (<https://land.copernicus.eu/pan-european/corine-land-cover/clc2018?tab=mapview>). Black dots with labels  
 153 (abbreviations explained in Table 1) represent sampled headwater streams and drainage ditch sampling points.  
 154 Wastewater inflows sampled are indicated by blue arrows on the maps. Drainage ditches in Loisach catchment  
 155 were dug in the 1930s to 1960s to lower water levels to improve grassland productivity in areas formerly  
 156 occupied by wetlands.



7

## 157 2.2 Sub-catchment delineation and land use classification

158 Sub-catchments for each sampling point in the Loisach, Goldersbach, Steinlach, Ammer and  
159 Schwingbach catchments were delineated in QGIS from a Digital Elevation Model (DEM) (EU-DEM v1.1) with  
160 a 25 m resolution (European Copernicus mission, retrieved August 1, 2021, [https://land.copernicus.eu/imagery-](https://land.copernicus.eu/imagery-in-situ/eu-dem/eu-dem-v1.1)  
161 [in-situ/eu-dem/eu-dem-v1.1](https://land.copernicus.eu/imagery-in-situ/eu-dem/eu-dem-v1.1)). Land use/ land cover percentages of all the delineated sub-catchments were  
162 calculated from Corine Land Cover 2018 survey with a 25 ha spatial resolution (retrieved August 1, 2021,  
163 <https://land.copernicus.eu/pan-european/corine-land-cover/clc2018?tab=mapview>). For the purposes of data  
164 analysis, we classified sub-catchments according to their dominant land cover (>50% of the total area) into forest  
165 (FOR), cropland (CRP), grassland (GRA), and wetland (WET), and further differentiated sub-catchments with  
166 influence of settlement areas (S) and wastewater inflows (W). (Table 1). As drainage ditches (DD) in the Loisach  
167 catchment were also added as extra land use category, this classification resulted in a total of 9 land use classes  
168 (for details see Table 1).

## 169 2.3 Hydrological and water physico-chemical characteristics

170 In the Loisach and Schwingbach catchments, discharge was calculated (Gore, 2007) from stream depth  
171 and velocity measurements using an electromagnetic sensor (OTT-MF-Pro, Hydromet, Germany). For streams in  
172 the Neckar sub-catchments, velocity was measured using the electromagnetic sensor (OTT-MF-Pro, Hydromet,  
173 Germany), and depth and discharge were obtained directly from gauging stations maintained by the water  
174 authority of the state of Baden-Württemberg (<https://udo.lubw.baden-wuerttemberg.de/public/index.xhtml>). The  
175 slope of a ~5 m reach at each sampling point was measured using a laser rangefinder with a slope function  
176 (Nikon Model: 8381, Japan). The slopes and velocities were used to model the site-specific gas transfer  
177 velocities ( $k$  in  $\text{m d}^{-1}$ ) for the quantification of daily GHG fluxes per unit stream surface area ( $\text{mass m}^{-2} \text{d}^{-1}$ ) (see  
178 details in the flux calculation section).

179 Discharge measurements at each sampling location and at every sampling event were complemented by  
180 *in situ* measurements of water temperature ( $^{\circ}\text{C}$ ), electrical conductivity ( $\mu\text{S cm}^{-1}$ ), dissolved oxygen (DO) ( $\text{mg L}^{-1}$ ),  
181 and pH using the Pro DSS multiprobe (YSI Inc., USA). Water samples for nutrient and organic carbon  
182 analyses were also collected and filtered on-site through polyethersulfone (PES) filters (0.45  $\mu\text{m}$  pore size, pre-  
183 leached with 60 ml of miliq water). The samples were stored in triplicates in 30 ml acid-washed HDPE sample  
184 bottles and transported within 24 h to the laboratories at Karlsruhe Institute of Technology, Campus Alpin,  
185 Justus Liebig University Giessen, or the University of Tübingen. On arrival, all samples were immediately  
186 frozen for later analysis.

187 After unfreezing the samples overnight in a  $4^{\circ}\text{C}$  refrigerator, the samples were directly analyzed for  
188 dissolved organic carbon (DOC), total dissolved nitrogen (TDN), nitrate ( $\text{NO}_3\text{-N}$ ), and ammonium ( $\text{NH}_4\text{-N}$ )  
189 concentrations. Dissolved organic nitrogen (DON) concentrations were estimated as the difference between the  
190 TDN and dissolved inorganic nitrogen DIN ( $\text{NO}_3\text{-N} + \text{NH}_4\text{-N}$ ) concentrations. DIN concentrations were  
191 determined using colorimetric methods, and the absorbance of the samples was measured using a microplate  
192 spectrophotometer (Model: Epoch, BioTek Inc., USA).  $\text{NO}_3\text{-N}$  concentrations were analyzed based on reactions  
193 with the Griess reagent (Patton & Kryskalla, 2011), and  $\text{NH}_4\text{-N}$  concentrations were analyzed using the  
194 indophenol method (Bolleter et al., 1961). The DOC concentrations were measured as non-purgeable organic



8

195 carbon (NPOC) using a TOC/ TN analyzer (Analytica-Jena; multi N/C 3100, Germany) after pre-treating the  
196 sample with 25% HCl acid to remove the dissolved inorganic carbon (DIC). The TDN concentrations were  
197 analyzed simultaneously with the same instrument (Analytica-Jena; multi N/C 3100, Germany).

#### 198 **2.4 Gas sampling, analysis, and calculations of annual areal fluxes**

199 GHG samples of stream, ditch and waste water were collected in triplicates simultaneously with the  
200 water physico-chemical samples using the headspace equilibration technique (Raymond et al., 1997). In brief, 80  
201 ml of background water was equilibrated with 20ml of atmospheric air in a syringe at *in situ* water temperatures,  
202 and the headspace gas sample transferred into 10ml glass vials for GHG concentration analysis in the laboratory  
203 of the Karlsruhe Institute of Technology, Campus Alpin (see full sampling details in Mwanake et al., 2022).  
204 Atmospheric air samples were taken twice (morning and afternoon) on each sampling day to correct for  
205 background atmospheric GHG concentrations. GHG concentrations from the headspace were analyzed using an  
206 SRI gas chromatograph (8610C, Germany) with an electron capture detector (ECD) for N<sub>2</sub>O and a flame  
207 ionization detector (FID) with an upstream methanizer for simultaneous measurements of CH<sub>4</sub> and CO<sub>2</sub>  
208 concentrations. Dissolved GHG concentrations in the stream water were calculated from post-equilibration gas  
209 concentrations in the headspace after correcting for atmospheric (ambient) GHG concentrations (e.g., Aho et al.,  
210 2019; Mwanake et al., 2022).

211 Daily diffusive fluxes ( $F$ ) (moles m<sup>-2</sup> d<sup>-1</sup>) of the GHGs were estimated using Fick's Law of gas  
212 diffusion, where the  $F$  is the product of the gas exchange velocity ( $k$ ) (m d<sup>-1</sup>) and the difference between the  
213 stream water ( $C_{aq}$ ) (moles m<sup>-3</sup>) and the ambient atmospheric gas concentration in water assuming equilibrium  
214 with the atmosphere ( $C_{sat}$ ) (moles m<sup>-3</sup>) (Equation 1). GHG concentrations and fluxes were expressed in mass  
215 units by multiplying by the respective molar masses.

$$216 \quad F = k (C_{aq} - C_{sat}) \quad (1)$$

217 The temperature-specific gas transfer velocities ( $k$ ) for each of the gases were calculated from  
218 normalized gas transfer velocities ( $k_{600}$ ) (m d<sup>-1</sup>) (corresponding to the  $k$  of CO<sub>2</sub> at 20° C with a Schmidt number  
219 of 600) and temperature-dependent Schmidt numbers ( $Sc$ ) (unit-less) of the respective gases (Equation 2).

$$220 \quad k = k_{600} \times \left( \frac{600}{Sc} \right)^{0.5} \quad (2)$$

221 The  $k_{600}$  was modeled using Equation 3 (drawn from equation 4 in Table 2 of Raymond et al. (2012)), which was  
222 calibrated from headwater streams of similar characteristic of our study sites, where  $V$  is stream velocity (m s<sup>-1</sup>)  
223 and  $S$  is the slope (m m<sup>-1</sup>).

$$224 \quad k_{600} = VS^{0.76} \times 951.5 \quad (3)$$

225 Before choosing the aforementioned equation for modeling the  $k_{600}$  values, we compared the  $k_{600}$  values  
226 calculated from all seven empirical models from Raymond et al 2012. The predicted  $k_{600}$  values from models  
227 3,4,5 and 6 in Table 2 of Raymond et al. (2012), which all use velocity and slope as input parameters, were  
228 mostly similar for the three discharge periods and across all stream orders 1–6 (ANOVA;  $p > 0.05$ ). In contrast,  
229 the calculated  $k_{600}$  values from equation 1, 2 and 7, which use a stream depth parameter, were higher (ANOVA;  
230  $p < 0.05$ ), particularly from the higher stream orders (5–6). This finding is inconsistent with the energy dissipation





9

231 model of turbulent streams where  $k_{600}$  is predicted to decrease with stream order. We therefore interpreted this to  
232 indicate a breakdown of these models for higher stream orders. This is also in agreement with recommendations  
233 from Raymond et al. 2012, and we therefore choose not to use models 1, 2 and 7 for this study. Out of the  
234 remaining equations 3, 4, 5 and 6, we used equation 4, which calculates  $k_{600}$  based on the slope and velocity  
235 parameters, and was also in line with several previous studies spanning a wide range of stream orders similar to  
236 our study. (See, Aho et al., 2019; Borges et al., 2019; Mwanake et al., 2019; Hall & Ulseth, 2020; Aho et al.,  
237 2021; Mwanake et al., 2022). The uncertainties in the modelled gas transfer velocities were reduced in this study  
238 by parametrization of the velocities and slopes based on actual field measurements of both variables. Equation 3  
239 was also used to estimate the gas transfer velocities in the drainage ditches that also had a measurable flow  
240 velocity and slope.

241 Water-to-atmosphere fluxes for all three GHGs across all land use classes in each subcatchment were  
242 calculated from the mean daily  $\text{CO}_2$ ,  $\text{CH}_4$  and  $\text{N}_2\text{O}$  fluxes during different discharge conditions. Total GHG  
243 fluxes were expressed as  $\text{CO}_2$  equivalents emissions ( $\text{mg CO}_2\text{-eq m}^{-2} \text{d}^{-1}$ ) computed from global warming  
244 potentials ( $\text{GWP}_{100}$ ) using 28 for  $\text{CH}_4$  and 298 for  $\text{N}_2\text{O}$  (IPCC, 2014). In order to scale tri-weekly measurements  
245 to annual flux estimates, we followed the procedure developed in Mwanake et al. (2022). Briefly, we classified  
246 each sampling date of every location into low, medium, or high discharge conditions according to whether  
247 normalized discharge fell in the 0–33% percentile (low), 34–66% (medium), or 67–100% (high) days.  
248 Normalized discharge for each site was determined by dividing each absolute discharge measurement for every  
249 site visit during the year with the maximum measured discharge. The number of days in each discharge period  
250 were estimated as the ratio of the number of observations in each discharge period to the total number of flux  
251 observations in individual land use classes in each catchment.  $\text{CO}_2$  equivalents fluxes were then calculated for  
252 the three different discharge periods in each land use class by multiplying the daily mean  $\text{CO}_2$  equivalents flux  
253 measured during each period and the number of days within each period. Annual fluxes were finally estimated  
254 by summing up the emissions of the low, medium, and high discharge periods for the individual land use classes  
255 in each catchment.



256 **2.5 Statistical analysis**

257 Linear mixed-effects models were used to investigate the effect of seasonality and land use on water  
258 physico-chemical variables, GHG concentrations, and fluxes ("lme4" package in R version 4.1.1). Fixed effects  
259 in the models consisted of land use classes in each catchment (Table 1) and seasons: summer June 1–August 31,  
260 autumn September 1–November 30, winter December 1–February 28, and spring March 1–31<sup>st</sup> May. Random  
261 effects accounting for repeated measures were also included in the models. Model performance was assessed  
262 based on the distribution of residuals (i.e. residuals should be normally distributed with a mean close to zero) and  
263 conditional  $r^2$  values calculated from significant models (p-value <0.05) ("MuMIn" package in R). A Tukey post-  
264 hoc test (p-value <0.05) of least-square means was used on the mixed models to identify individual differences  
265 within each categorical fixed effect. GHG concentration and flux data and other water physico-chemical  
266 variables were transformed using the natural logarithm to meet the assumption of normality. Because we  
267 quantified occasional negative fluxes in some of our sites, constant flux values of 50 mg m<sup>-2</sup> d<sup>-1</sup> for CO<sub>2</sub>-C, 0.5  
268 mg m<sup>-2</sup> d<sup>-1</sup> for CH<sub>4</sub>-C, and 10 µg m<sup>-2</sup> d<sup>-1</sup> for N<sub>2</sub>O-N were added to the fluxes to enable the natural logarithm  
269 transformations.

270 Path analysis from structural equation models (SEMs, "lavaan" package in R version 4.1.1) were used to  
271 determine how environmental factors linked to seasonality and landuse, directly or indirectly influenced *in*  
272 *stream* GHG production and consumption processes as well as external GHG sources, i.e., dissolved GHGs  
273 inputs to the streams originating from either wastewater inflows or terrestrial landscapes which were not  
274 produced *in situ*. In brief, these SEMs were constructed on the basis of causal relationships between exogenous  
275 variables (interpreted as ultimate drivers of GHG concentrations) and endogenous variables, which are affected  
276 by the exogenous variables and also act as immediate drivers that affect GHG concentrations. Endogenous  
277 variables in the models, which are known to influence *in situ* biogeochemical GHG production and consumption  
278 processes directly, included dissolved oxygen DO (% saturation), DOC (mg L<sup>-1</sup>), NH<sub>4</sub>-N (mg L<sup>-1</sup>), and NO<sub>3</sub>-N  
279 (mg L<sup>-1</sup>) concentrations (Battin et al., 2008; Stanley et al., 2016; Quick et al., 2019). The exogenous variables in  
280 the models, which influence *in situ* GHG concentrations either directly by facilitating dissolved GHG inputs or  
281 indirectly by controlling the endogenous variables, were water temperature (°C) (a proxy for different seasons),  
282 stream velocity V (m s<sup>-1</sup>), % upstream agricultural area for each sampling point (AGR: grassland + cropland  
283 area) and wastewater inflows (WW: Boolean numbers, i.e., 1 for the presence of wastewater inflow and 0 for  
284 absence).

285 The hypothesized relationships between the endogenous and exogenous drivers of instream GHG  
286 concentrations were assessed in the overall theoretical SEM, which is made up of several multivariate regression  
287 equations shown in Equations 4-8. To get the best-fit SEM, removal of parts of the theoretical SEM was done  
288 manually until the model with the highest parsimony fit index (PNFI), and a root mean squared error of  
289 approximation (RMSEA) of <=0.05 was found (Schumacker and Lomax, 2016). Graphical representations of the  
290 significant relationship pathways from the best-fit model, including standardized slope parameter estimates, were  
291 done using the "semPlot" package in R software.

292 
$$\text{Log}_e \text{GHG concentration} = \text{DO} + \text{DOC} + \text{stream velocity} + \text{water temperature} + \text{Log}_e \text{NO}_3 +$$
  
293 
$$\text{Log}_e \text{NH}_4 + \text{wastewater inflow} + \text{agricultural area}$$
  
294 (4)



11

295  $\text{Log}_e \text{NO}_3 = \text{DO} + \text{Log}_e \text{NH}_4 + \text{DOC} + \text{wastewater inflow} + \text{agricultural area} +$   
296  $\text{stream velocity}$  (5)

297  $\text{Log}_e \text{NH}_4 = \text{DO} + \text{DOC} + \text{wastewater inflow} + \text{agricultural area} +$   
298  $\text{stream velocity}$  (6)

299  $\text{DOC} = \text{wastewater inflow} + \text{agricultural area} + \text{stream velocity}$  (7)

300  $\text{DO} = \text{DOC} + \text{wastewater inflow} + \text{agricultural area} + \text{stream velocity}$  (8)



Table 1: Summary descriptions of sampling sites located in the Schwingbach, Loissach, and Neckar sub-catchments (Goldersbach, Ammer and Steinlach) (Fig. 1). The land use (%) was calculated for the site-specific upstream sub-catchments based on the Corine Land Cover 2018 survey of Europe (See main text for details).

Main Catchment	Site	Stream order	Coordinates (decimal degrees)		Sub-catchment area (Ha)	Elevation at sampling point	Sub-catchment Landuse / Landcover (%)			Wastewater inflow	Main sub-catchment landuse class			Main land use Abbreviations
			Latitude	Longitude			Forest	Wetland	Grassland		Cropland	Urban	Wetland	
Loissach	Stream	1	47.5694	11.1554	4	651	40	60	0	0	0	0	Wetland	WET
Loissach	Stream	2	47.5689	11.1556	10	645	22	78	0	0	0	0	Wetland	WET
Loissach	Stream	1	47.5440	11.1193	11	660	0	0	100	0	0	0	Grassland	GRA
Loissach	Stream	1	47.5399	11.1105	13	663	19	0	81	0	0	0	Grassland	GRA
Loissach	Stream	1	47.4670	11.0537	40	750	86	0	14	0	0	0	Forest	FOR
Loissach	Stream	2	47.4691	11.0394	75	756	99	0	0	0	1	0	Forest	FOR
Loissach	Stream	2	47.5858	11.1429	102	719	100	0	0	0	0	0	Forest	FOR
Loissach	Drainage ditch		47.5963	11.1730	11	630	27	0	73	0	0	0	Drainage ditch	DD
Loissach	Drainage ditch		47.5953	11.1657	11	645	43	57	0	0	0	0	Drainage ditch	DD
Loissach	Drainage ditch		47.5696	11.1550	17	630	47	0	53	0	0	0	Drainage ditch	DD
Schwingbach	Stream	1	50.5051	8.6127	41	297	96	0	0	4	0	0	Forest	FOR
Schwingbach	Stream	1	50.4695	8.6179	60	187	0	0	0	100	0	0	Cropland	CRP
Schwingbach	Stream	2	50.4811	8.5407	62	241	98	0	2	0	0	0	Forest	FOR
Schwingbach	Stream	1	50.4756	8.5472	67	334	86	0	0	14	0	0	Forest	FOR
Schwingbach	Stream	2	50.4922	8.5971	220	260	47	0	0	53	0	0	Cropland	CRP
Schwingbach	Stream	2	50.5032	8.5553	220	272	65	0	0	35	0	0	Forest	FOR
Schwingbach	Stream	2	50.4887	8.5555	268	204	83	0	0	17	0	0	Forest	FOR
Schwingbach	Stream	1	50.4669	8.5792	355	207	14	0	0	84	2	0	Cropland	CRP
Schwingbach	Stream	3	50.5050	8.6148	2337	183	37	0	6	48	9	0	Cropland+settlement	CRP_S
Schwingbach	Stream	3	50.5166	8.5992	5345	189	44	0	4	45	7	0	Cropland+settlement	CRP_S
Goldersbach (Neckar)	Stream	5	48.5588	9.0591	11623	367	97	0	0	3	0	0	Forest	FOR
Ammer (Neckar)	Stream	5	48.5649	8.8986	26157	379	11	0	1	84	4	0	Cropland+settlement	CRP_S
Ammer (Neckar)	Stream	6	48.5640	8.8997	26361	377	11	0	1	83	5	Yes	Cropland+settlement+wastewater	CRP_S_W
Ammer (Neckar)	Stream	6	48.5271	8.9615	30441	348	14	0	2	77	8	No	Cropland+settlement	CRP_S
Steinlach/Neckar	Stream	6	48.4796	9.0634	51332	348	74	0	10	11	4	No	Forest+settlement	FOR_S
Steinlach/Neckar	Stream	6	48.4812	9.0639	51332	344	74	0	10	11	4	Yes	Forest+settlement+wastewater	FOR_S_W
Ammer/Neckar	Wastewater effluent		48.5644	8.8993									Wastewater	WWA
Steinlach/Neckar	Wastewater effluent		48.4805	9.0636									Wastewater	WWS



13

302 **3 Results**

303 **3.1 Hydrological variables**

304 Across all sampling points and seasons, tri-weekly sampled stream velocity measurements (annual  
305 mean  $\pm$  SE) were two-folds higher for streams ( $0.19 \pm 0.009 \text{ m s}^{-1}$ , range: 0.01- 1.17) than ditches ( $0.05 \pm 0.06 \text{ m}$   
306  $\text{s}^{-1}$ , range: 0.01–0.23) (Fig A1). Seasonality had an overall significant effect on stream velocities across all  
307 sampling points, with higher stream velocities observed in spring ( $0.24 \pm 0.02 \text{ m s}^{-1}$ ) than in autumn ( $0.12 \pm 0.01$   
308  $\text{m s}^{-1}$ ) (Table 2; Table B2). Discharge in streams ( $3.9\text{--}18,500 \text{ L s}^{-1}$ ) and in ditches ( $0.1\text{--}37 \text{ L s}^{-1}$ ) was highly  
309 variable, reflecting differing stream sizes and seasonal variability (Fig. A1). The Neckar sub-catchments,  
310 dominated by streams (orders 5 - 6 ), had an order of magnitude higher mean annual discharge ( $874.7 \pm 178 \text{ L s}^{-1}$ )  
311 than the streams in the other catchments (Loisach:  $50.5 \pm 6 \text{ L s}^{-1}$  and Schwingbach:  $26.7 \pm 4 \text{ L s}^{-1}$ ). The  
312 average discharge at the stream and ditch sampling points in all our study catchments were 3 to 5-fold higher in  
313 spring and summer ( $384.1 \pm 96$  and  $526.4 \pm 171 \text{ L s}^{-1}$ , respectively) than in autumn and winter ( $86.25 \pm 13.07$   
314 and  $157.3 \pm 31.58$ , respectively; Table 2; Table B2).



14

315 Table 2: Results of multiple linear mixed-effects models predicting the effect of seasonality (summer, autumn,  
 316 winter, and spring) and sub-catchment land use (Table 1) on stream velocity, discharge, water physico-chemical  
 317 variables, GHG concentration, gas-transfer velocity, and GHG flux. The model performance was assessed based  
 318 on conditional  $r^2$  and the distribution of residuals, including the variances explained by fixed effects and repeated  
 319 mea sures' random effects.

Dependent variables	Conditional $r^2$	Type 2 ANOVA table	
		Season (df=3)	Land use (df=11)
		F-statistic/significance	F-statistic/significance
<b>Water physico-chemical and hydrological variables</b>			
Temperature ( $^{\circ}$ C)	0.87	66.3***	9.1***
pH	0.80	3.1*	97.8***
DO ( $\text{mg L}^{-1}$ )	0.83	20.1***	143.7***
Electrical Conductivity ( $\mu\text{s cm}^{-1}$ )	0.83	4.9**	86.1***
$\text{NO}_3\text{-N}$ ( $\text{mg L}^{-1}$ ) <sup>a</sup>	0.80	4.9**	141***
$\text{NH}_4\text{-N}$ ( $\text{mg L}^{-1}$ ) <sup>a</sup>	0.60	ns	32.3***
TDN ( $\text{mg L}^{-1}$ ) <sup>a</sup>	0.79	5.6**	93.8***
DON ( $\text{mg L}^{-1}$ ) <sup>a</sup>	0.55	ns	13.9***
DOC ( $\text{mg L}^{-1}$ ) <sup>a</sup>	0.59	ns	47.3***
DOC:DIN	0.84	3.2*	133.2***
DOC:DON	0.63	ns	15.1***
Velocity <sup>a</sup>	0.59	3.7*	34.5***
Discharge <sup>a</sup>	0.86	4.6**	96.9***
<b><math>k_{600}</math>, Gas concentration and flux</b>			
$\text{CO}_2\text{-C}$ concentration ( $\mu\text{g L}^{-1}$ ) <sup>a</sup>	0.86	25.6***	219.3***
$\text{CH}_4\text{-C}$ concentration ( $\mu\text{g L}^{-1}$ ) <sup>a</sup>	0.89	ns	273.1***
$\text{N}_2\text{O-N}$ concentration ( $\text{ng L}^{-1}$ ) <sup>a</sup>	0.75	3.3*	69***
$k_{600}$ ( $\text{m d}^{-1}$ ) <sup>a</sup>	0.57	ns	31.2***
$\text{CO}_2\text{-C}$ flux ( $\text{mg m}^{-2} \text{d}^{-1}$ ) <sup>a</sup>	0.57	ns	50.2***
$\text{CH}_4\text{-C}$ flux ( $\text{mg m}^{-2} \text{d}^{-1}$ ) <sup>a</sup>	0.79	ns	113***
$\text{N}_2\text{O-N}$ flux ( $\mu\text{g m}^{-2} \text{d}^{-1}$ ) <sup>a</sup>	0.70	3.9*	75.6***
Total fluxes $\text{CO}_2\text{-eq}$ ( $\text{g m}^{-2} \text{d}^{-1}$ ) <sup>a</sup>	0.67	ns	67***
Level of significance (p-value)	<sup>a</sup> Natural logarithm transformation		
* <0.05			
** <0.01			
*** <0.001	Conditional $r^2$ = Variance explained by fixed and random effects of sampling date		
ns >0.05	df= degrees of freedom		

320

321

322

### 323 3.2 Water physico-chemical variables

#### 324 3.2.1 Seasonal variation

325 Water temperature, DO, and pH ranged from 0.9–24 $^{\circ}$  C, 1.1–15.7  $\text{mg O}_2 \text{L}^{-1}$ , and 6.7–9.0, respectively.  
 326 Streams in the mountainous Loisach catchment had a mean annual ( $\pm$  SE) water temperature of  $9.0 \pm 0.2$   $^{\circ}$  C,  
 327 which was  $\sim 1$   $^{\circ}$  C colder than streams of the Schwingbach catchment ( $10.0 \pm 0.4$   $^{\circ}$  C) and 3 degrees colder than



328 streams in the Neckar sub-catchments ( $12.0 \pm 0.3$  °C). The annual ranges of  $\text{NH}_4\text{-N}$ ,  $\text{NO}_3\text{-N}$ , DON, TDN, and  
329 DOC concentrations across all catchments were  $0.05\text{--}1.0$   $\text{mg L}^{-1}$ ,  $0.5\text{--}14.8$   $\text{mg L}^{-1}$ ,  $0.05\text{--}10.9$   $\text{mg L}^{-1}$ ,  $0.6\text{--}17.0$   
330  $\text{mg L}^{-1}$ , and  $0.9\text{--}16.0$   $\text{mg C L}^{-1}$ , respectively. DO,  $\text{NO}_3$ , and TDN concentrations showed significant seasonal  
331 variability (Table 2, Table B2). DO was higher in winter and spring than in summer and autumn.  $\text{NO}_3\text{-N}$  and  
332 TDN concentrations were highest in winter and lowest in autumn and summer, while  $\text{NH}_4\text{-N}$ , DOC and DON  
333 showed no significant seasonal variation (Table 2; Table B2). We additionally calculated DOC:DIN and  
334 DOC:DON molar ratios, which had interquartile ranges from  $0.9\text{--}4.9$  and  $4.1\text{--}29.0$ , respectively. DOC:DIN  
335 ratios showed significant seasonal variability, with higher values in summer and spring than in winter, while no  
336 seasonal variability was found for DOC:DON ratios (Table 2: Table B2).

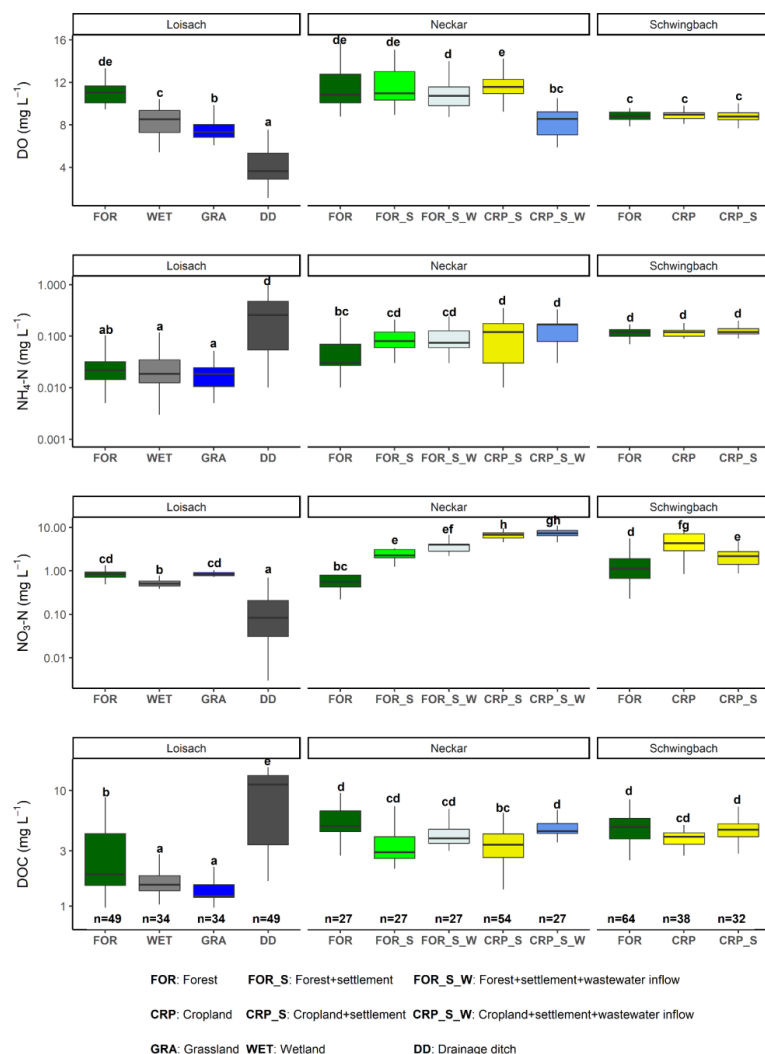
### 337 3.2.2 Land use variation

338 Catchment land use was more significant than seasonality in explaining the variability of most water  
339 physico-chemical variables (Table 2). In the Loisach catchment, ditches had up to 2.6 times lower DO and up to  
340 8 times lower  $\text{NO}_3\text{-N}$  concentrations than the streams across all land use types (Fig. 2; Table B3). In contrast,  
341  $\text{NH}_4\text{-N}$  and DOC concentrations, as well as the DOC:DIN ratio were 6-10 times higher in the ditches than in the  
342 streams (Fig. 2; Table B3). In the Neckar sub-catchments, forested streams had 1-2 times higher DO and DOC  
343 concentrations than cropland, settlement, and wastewater-influenced streams. The opposite was true for  $\text{NO}_3\text{-N}$   
344 and DON concentrations, which were an order of magnitude higher in the cropland, settlement, and wastewater-  
345 influenced streams than in the forested streams (Fig. 2; Table B3). As a result, DOC:DIN and DOC:DON ratios  
346 in the Neckar sub-catchments were therefore higher in forested streams than in cropland, settlement, and  
347 wastewater-influenced streams (Table B3).

348 In addition, cropland streams directly receiving wastewater inflows also had significantly lower DO and  
349 higher DOC than cropland streams without wastewater inflows (Fig. 2; Table B3). While  $\text{NO}_3\text{-N}$  and DON  
350 concentrations were not significantly different in cropland streams with or without wastewater inflows, the  
351 concentrations of both variables was slightly higher in cropland streams with wastewater inflows (Table B3). In  
352 streams of the Schwingbach catchment, surrounding croplands and settlement areas also influenced  $\text{NO}_3\text{-N}$   
353 concentrations, which were up to 3-fold higher than in the forested streams. Across all the three catchments, DO  
354 concentrations, DOC:DIN and DOC:DON ratios were higher in the forested streams and decreased in streams of  
355 sub-catchments with predominant agricultural land uses or settlement areas, while the opposite was found for  
356  $\text{NO}_3\text{-N}$  and DON concentrations (Table B3). Additionally, forested streams in the Loisach catchment had an  
357 order of magnitude higher DOC:DON ratios than forested streams in the Neckar and Schwingbach catchments  
358 (Table B3).



16



359

360 Fig. 2: Boxplots of DO, NH<sub>4</sub>-N, NO<sub>3</sub>-N, and DOC concentrations in stream and ditch waters in the three  
 361 catchments grouped by dominating land uses (see Table 1 methods). Letters on top of the boxplots represent  
 362 significant differences ( $p < 0.05$ ) among land use classes across the three catchments based on Tukey post-hoc  
 363 analyses from the linear mixed-effects model results (Table 2).

364

### 365 3.3 GHG concentrations and fluxes

#### 366 3.3.1 Seasonal variation

367 In all headwater streams, CH<sub>4</sub> and N<sub>2</sub>O concentrations varied greatly, spanning three orders of  
 368 magnitude, i.e., from 0.03–58 μg-C L<sup>-1</sup> ( $p\text{CH}_4$  1.3–2,145 μatm) for CH<sub>4</sub> and from 20–18,717 ng-N L<sup>-1</sup> ( $p\text{N}_2\text{O}$ )





17

369 21– 15,813 natm) for N<sub>2</sub>O. In contrast, CO<sub>2</sub> concentrations varied less, spanning only one order of magnitude  
370 from 219–4,868 µg-C L<sup>-1</sup> (*p*CO<sub>2</sub> 369–7,979 µatm). GHG concentrations in ditches also varied widely, with CH<sub>4</sub>,  
371 N<sub>2</sub>O and CO<sub>2</sub> concentrations spanning 1-2 orders of magnitude ranging from 27–831 µg-C L<sup>-1</sup> (*p*CH<sub>4</sub> 1,469–  
372 34,482 µatm), 56–1,540 ng-N L<sup>-1</sup> (*p*N<sub>2</sub>O 35–1,512 natm), and 1,722– 9,746 µg-C L<sup>-1</sup> (*p*CO<sub>2</sub> 2,888–13,400  
373 µatm), respectively (Fig. A2–A5).

374 Streams and drainage ditches across all seasons were predominantly sources of atmospheric CH<sub>4</sub>, N<sub>2</sub>O,  
375 and CO<sub>2</sub>, as indicated by concentrations mostly above atmospheric background and the positive flux values  
376 displayed in Figure 3. CO<sub>2</sub> fluxes from streams ranged from -0.05–179 g C m<sup>-2</sup> d<sup>-1</sup> (mean 19 g C m<sup>-2</sup> d<sup>-1</sup>), CH<sub>4</sub>  
377 fluxes ranged from -0.40–325 mg C m<sup>-2</sup> d<sup>-1</sup> (mean 30 mg C m<sup>-2</sup> d<sup>-1</sup>), and N<sub>2</sub>O fluxes ranged from -9.2–199.5 mg  
378 N m<sup>-2</sup> d<sup>-1</sup> (mean 12 mg N m<sup>-2</sup> d<sup>-1</sup>). CO<sub>2</sub> and CH<sub>4</sub> fluxes from the ditches varied between 2–63 g C m<sup>-2</sup> d<sup>-1</sup> (mean  
379 13.7 g C m<sup>-2</sup> d<sup>-1</sup>) and from 117–7,933 mg C m<sup>-2</sup> d<sup>-1</sup> (mean 1,532 mg C m<sup>-2</sup> d<sup>-1</sup>), respectively, while N<sub>2</sub>O fluxes  
380 ranged from -0.8–7.1 mg N m<sup>-2</sup> d<sup>-1</sup> (mean 1.2 mg N m<sup>-2</sup> d<sup>-1</sup>).

381 Seasonal variation in GHG concentrations and fluxes were GHG dependent and varied across the  
382 different land uses within each catchment (Fig. 3; Fig. A2, A3, and A4). In the Loisach catchment, there was a  
383 decline in *instream* CO<sub>2</sub> concentrations in the summer followed by a subsequent increase in autumn, particularly  
384 at non-forested sampling points (Fig. A2). Similar *instream* CO<sub>2</sub> concentration trends with lower values in the  
385 summer season and increasing values in autumn, were also found for non-forested streams of the Neckar sub-  
386 catchments (Fig. A3). However, non-forested streams of the Schwingbach catchments showed slightly different  
387 trends, with a decline of CO<sub>2</sub> concentrations in spring and an increase of CO<sub>2</sub> concentrations in the late summer  
388 season. (Fig. A4). Considering all data over all catchments, seasonality had an overall significant effect (*p*<0.05)  
389 with CO<sub>2</sub> concentrations in summer being 1.6 times lower than in autumn, while CO<sub>2</sub> fluxes showed no  
390 significant seasonal variability (Table 2; Table B2).

391 In contrast to CO<sub>2</sub>, N<sub>2</sub>O concentrations in the Loisach and Schwingbach catchments decreased from  
392 summer to autumn but increased again towards the beginning of the winter season (Fig. A2, A4). In autumn,  
393 N<sub>2</sub>O concentrations at first and second order forested streams in the Loisach and Schwingbach catchments were  
394 often below atmospheric concentrations (Fig. A2, A4), characterizing these sites as N<sub>2</sub>O sinks (Fig. 2). A similar  
395 autumn decline in N<sub>2</sub>O concentrations was not observed in the streams of the Neckar sub-catchments, but rather,  
396 N<sub>2</sub>O concentrations increased from autumn to winter (Fig. A3). Across all catchments and sampling points, N<sub>2</sub>O  
397 concentrations were 2.4 times higher in winter than in the other seasons (Table B2). N<sub>2</sub>O fluxes were up to 1.6  
398 times higher in summer and winter than in autumn and spring (Fig. 3; Table B2), which represented periods of  
399 either high N<sub>2</sub>O concentrations and moderate gas transfer velocities (winter) or moderate N<sub>2</sub>O concentrations and  
400 high gas transfer velocities (summer) (Table B2).

401 CH<sub>4</sub> concentrations showed a seasonal pattern only in the Schwingbach catchment (Fig. A4), which  
402 showed a decline from summer through autumn and winter. This trend was not observed for the other  
403 catchments (Fig. A2, A3) and resulted in non-significant seasonal effect on both concentrations and fluxes when  
404 all data from all catchments were considered together (Table 2; Table B2). Overall, strong seasonal trends of  
405 GHG fluxes throughout the year were mostly found in human-influenced land use classes such as streams and



406 ditches in grasslands, croplands, and settlement areas, but not at streams whose sub-catchments were dominated  
 407 by forests or wetlands (Fig. 3).

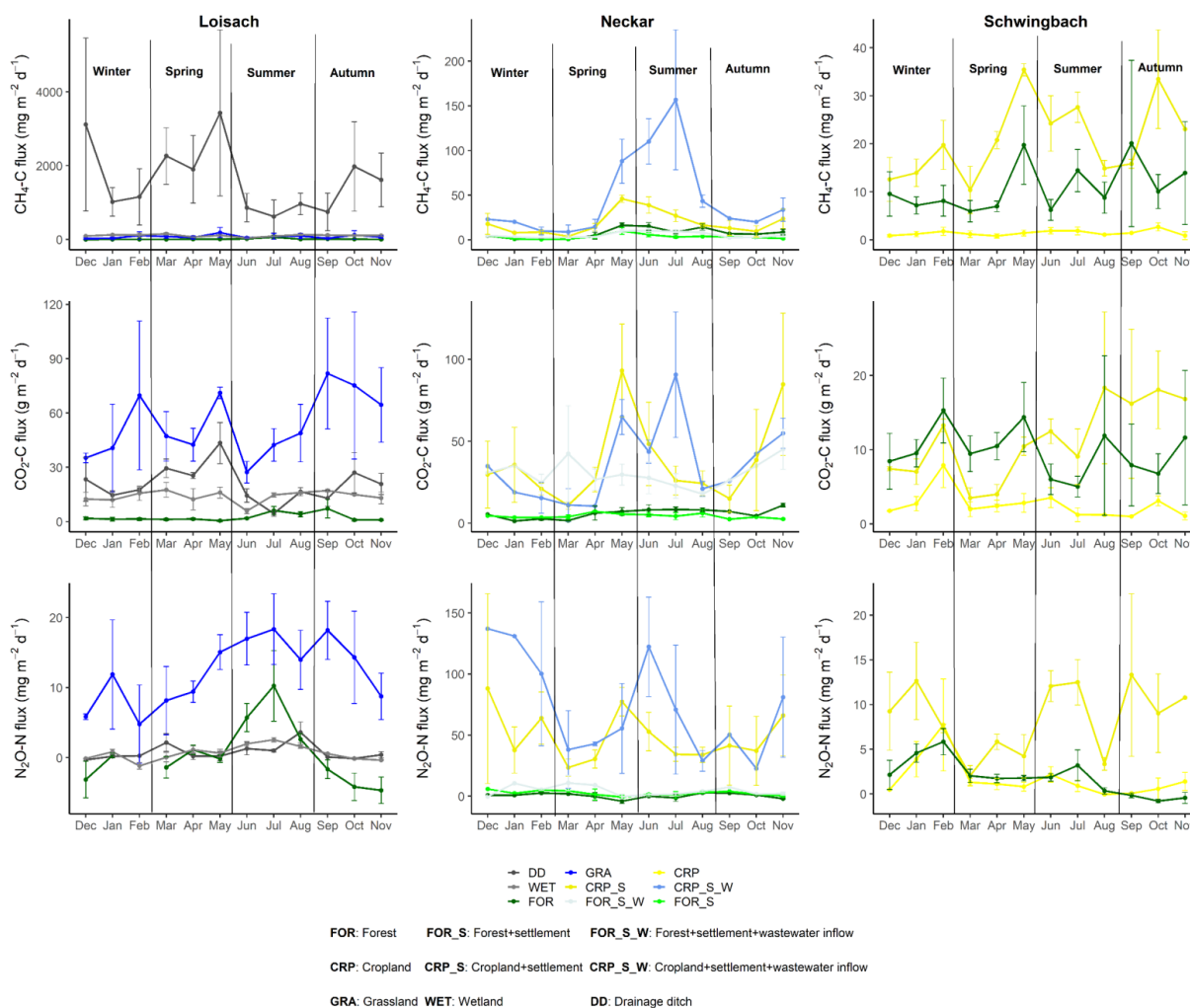


Fig. 3: Monthly mean  $\pm$  SE of  $\text{CO}_2$ ,  $\text{CH}_4$ , and  $\text{N}_2\text{O}$  fluxes across all 26 sampled streams and ditches in the Loisach, Neckar, and Schwingbach catchments (see Table 1 methods). The colors of the lines and labels on the graph indicate the nine dominant land use classes.

408 **3.3.2 Land use variation**

409 Similar to water physico-chemical variables, the variability in GHG concentrations and fluxes was  
 410 more strongly linked to catchment land use than seasonality (Table 2). In the Loisach catchment,  $\text{CO}_2$   
 411 concentrations and fluxes were an order of magnitude higher for the ditch and stream sites that were dominated



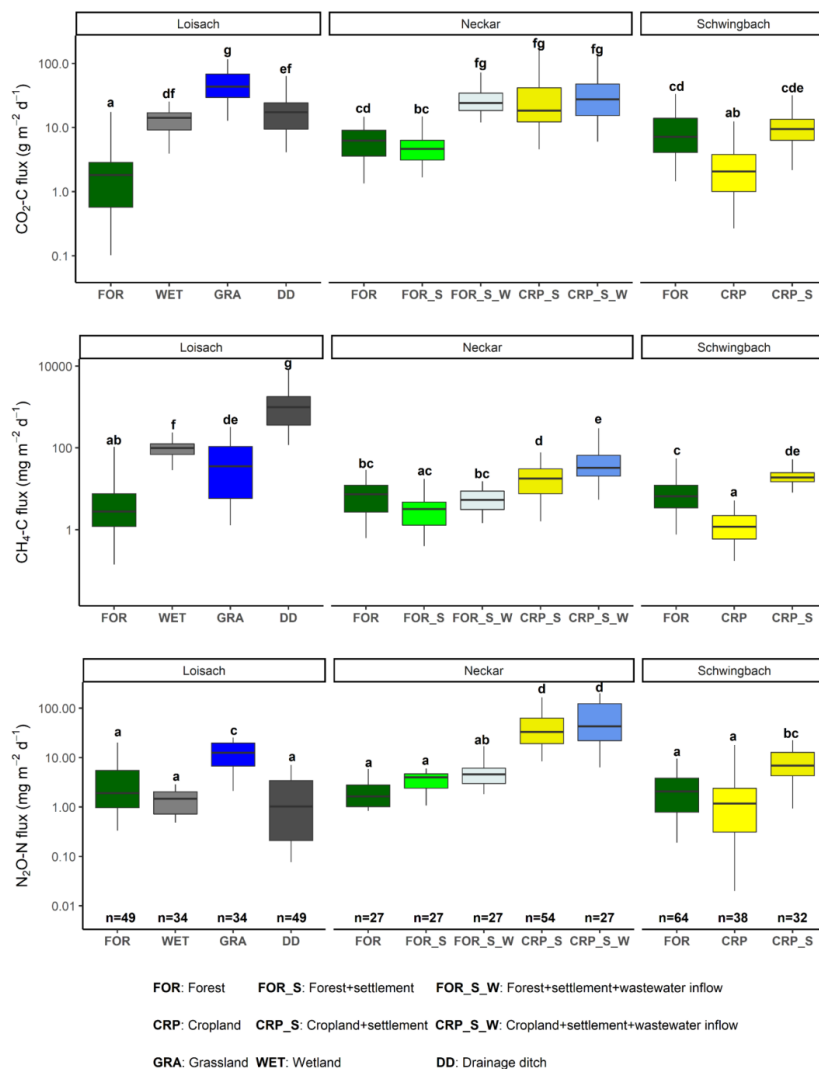
412 by grassland land uses than forested-dominated sites (Fig. 3; Fig. 4; Table B3). N<sub>2</sub>O concentrations and fluxes in  
413 streams were also an order of magnitude higher in the grassland streams compared to the wetland and forested  
414 ones, with the latter functioning as occasional sinks for atmospheric N<sub>2</sub>O (Fig. 3; Fig. 4; Table B3). Wetland  
415 streams had higher CH<sub>4</sub> fluxes than the other stream sites (Fig. 3; Fig. 4; Table B3). Overall, ditches showed up  
416 to 14 times higher CO<sub>2</sub> and up to 850 folds higher CH<sub>4</sub> concentrations than the streams of Loisach catchment  
417 (Fig. A5; Table B3). In contrast, N<sub>2</sub>O concentrations in the ditches were highly variable, with both higher and  
418 lower than atmospheric concentrations over the sampling year (Fig. A2). CH<sub>4</sub> fluxes were two orders of  
419 magnitude higher in ditches than in streams (Fig. 3; Fig. 4; Table B3). Interestingly, the ditches were even more  
420 often N<sub>2</sub>O sinks than forests, which resulted in overall lowest N<sub>2</sub>O fluxes e.g. 10 times lower than the ones of  
421 grassland-dominated streams (Fig. 3; Table B3)

422 In the Neckar sub-catchments, CO<sub>2</sub>, CH<sub>4</sub> and N<sub>2</sub>O concentrations and fluxes were 1-10 times higher in  
423 the streams located in cropland and settlement areas as compared to streams in forested areas (Fig. 3; Fig. 4; Fig.  
424 A5; Table B3). Generally, GHG concentrations and fluxes of streams in cropland and settlement areas further  
425 increased if sampling points were affected by wastewater inflows (Fig. 3; Fig. 4; Fig. A5; Table B3). For the  
426 latter, it is noteworthy that pronounced differences in wastewater characteristics existed in our study, even  
427 though the treatment procedures and the number of served households (80000) were comparable for the two  
428 wastewater treatment plants. Overall, the wastewater outflow in the Ammer catchment had higher TDN, DOC,  
429 CH<sub>4</sub> and N<sub>2</sub>O concentrations than the one in the Steinlach catchment (Table B1).

430 In contrast to the other two catchments, forested streams in the Schwingbach catchment had CO<sub>2</sub> and  
431 CH<sub>4</sub> concentrations and fluxes comparable to cropland and settlement-influenced streams within the catchment  
432 (Fig. 3; Fig. 4; Fig. A5; Table B3). However, N<sub>2</sub>O concentrations and fluxes were higher in streams with  
433 cropland and settlement influences than in forested streams (Fig. 3; Fig. 4; Fig. A5; Table B3).



20



434

435 Fig. 4: Boxplots of CO<sub>2</sub>, CH<sub>4</sub>, and N<sub>2</sub>O fluxes in stream and ditch waters in the three catchments grouped by land  
 436 uses (see Table 1 methods). Letters on top of the boxplots represent significant differences (p<0.05) amongst the  
 437 land use classes across the three catchments based on Tukey post-hoc analyses from the linear mixed-effects  
 438 models' results (Table 2).



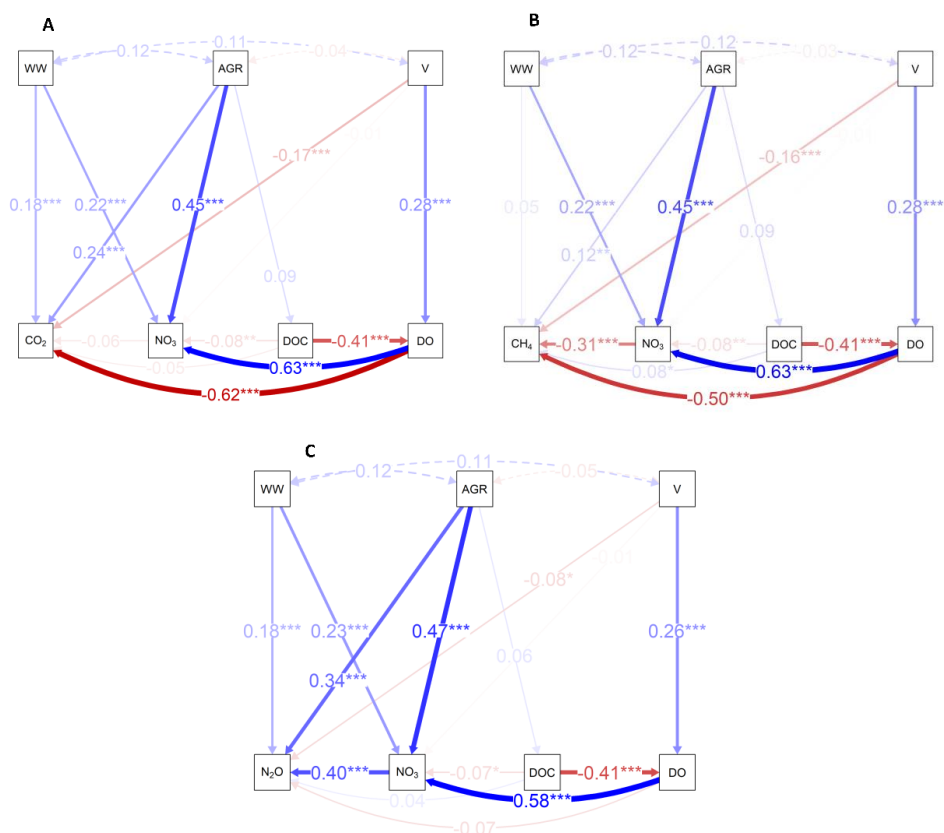
439 **3.4 Direct and indirect drivers of greenhouse gas concentrations**

440 We used path analyses from SEMs based on all our dataset in order to explain how indirect factors such  
441 as upstream agricultural area, wastewater inflow and stream velocity controlled the spatial-temporal dynamics of  
442 GHG concentrations that drove the fluxes. The slopes parameter estimates from the SEMs revealed significant  
443 ( $p < 0.05$ ) interactions between the aforementioned indirect drivers and DO (% saturation), DOC  $\text{mg L}^{-1}$  and  $\text{NO}_3\text{-}$   
444  $\text{N mg L}^{-1}$ , i.e. drivers that directly control *in situ* GHG concentrations (Fig. 5, Table B4). An increase in  
445 upstream agricultural area resulted in a ~45% increase in *in situ*  $\text{NO}_3\text{-N}$  concentrations. Wastewater inputs  
446 resulted in a ~22% increase in *in situ*  $\text{NO}_3$  concentrations, while DOC concentrations were not significantly  
447 affected. DO decreased with increasing DOC concentrations, while  $\text{NO}_3\text{-N}$  concentrations followed an opposite  
448 pattern and increased with increasing DO concentrations (Fig 5).

449  $\text{CO}_2$  and  $\text{CH}_4$  concentrations had a negative relationship with DO (Fig 5A-B), but  $\text{N}_2\text{O}$  concentrations  
450 were not significantly related to DO (Fig 5C). Besides DO,  $\text{CO}_2$  concentrations decreased by 17% with stream  
451 velocity, and increased by 18% with wastewater inflows and by 24% with increasing upstream agricultural area  
452 (Fig 5A).  $\text{CH}_4$  concentrations also decreased by 16% with increasing stream velocity. However, the effect of  
453 wastewater inflows (+5%) or increased share of agricultural areas (+12%) on  $\text{CH}_4$  concentrations was lower than  
454 for  $\text{CO}_2$ . Additionally,  $\text{CH}_4$  concentrations also decreased by 31% with increasing  $\text{NO}_3\text{-N}$  concentrations (Fig.  
455 5B). In contrast to  $\text{CO}_2$  and  $\text{CH}_4$ ,  $\text{N}_2\text{O}$  concentrations increased by 40% with increasing  $\text{NO}_3\text{-N}$  concentrations,  
456 while the effect of stream velocity was of minor importance (-8%). Compared to  $\text{CH}_4$  and  $\text{CO}_2$ ,  $\text{N}_2\text{O}$   
457 concentrations in stream and river waters showed similar or stronger relationships to wastewater inflows (+18%)  
458 and upstream agricultural area (+34%) (Fig 5C). Overall, the best-fit SEMs explained 60, 66, and 46 % of the  
459 observed variances in  $\text{CO}_2$ ,  $\text{CH}_4$ , and  $\text{N}_2\text{O}$  concentrations, respectively (Table B4)



22



460

461

462 Fig. 5: Regression pathways predicting A)  $\text{Log}_e \text{CO}_2$  concentration  $\mu\text{g-C L}^{-1}$ , B)  $\text{Log}_e \text{CH}_4$  concentration  $\mu\text{g-C L}^{-1}$  and C)  $\text{Log}_e \text{N}_2\text{O}$  concentration  $\text{ng-N L}^{-1}$  across all sampling points and seasons from best-fit SEMs consisting of endogenous (DO, DOC, and  $\text{NO}_3\text{-N}$ ) and exogenous variables (stream velocity (V), percentage agricultural area (AGR; grassland+cropland areas), and wastewater inflows (WW)). The numbers on the lines represent standardized slope parameters, with significant relationships indicated by \*. Solid lines represent actual fitted relationships, while dashed lines represent co-variances in the exogenous variables. Blue lines represent positive relationships and red represents negative relationships, with width and color intensity representing the strength of the relationships.

470 **3.5 Annual areal fluxes**

471 Based on global warming potential calculations,  $\text{CO}_2$  dominated the annual GHG emissions across all  
 472 headwater streams, with contributions ranging from 56 %–100%. The non- $\text{CO}_2$  gasses' contributions were much  
 473 lower and ranged from 0–43% for  $\text{CH}_4$  and 0–21% for  $\text{N}_2\text{O}$  (Fig. 6). The highest contribution of  $\text{CH}_4$  (43%) was  
 474 found at ditch sampling points in the Loisach, while the highest  $\text{N}_2\text{O}$  contributions (up to 21%) were observed at  
 475 the cropland-influenced streams fed by wastewater inflows in the Neckar sub-catchments (Fig. 6). Overall, the



23

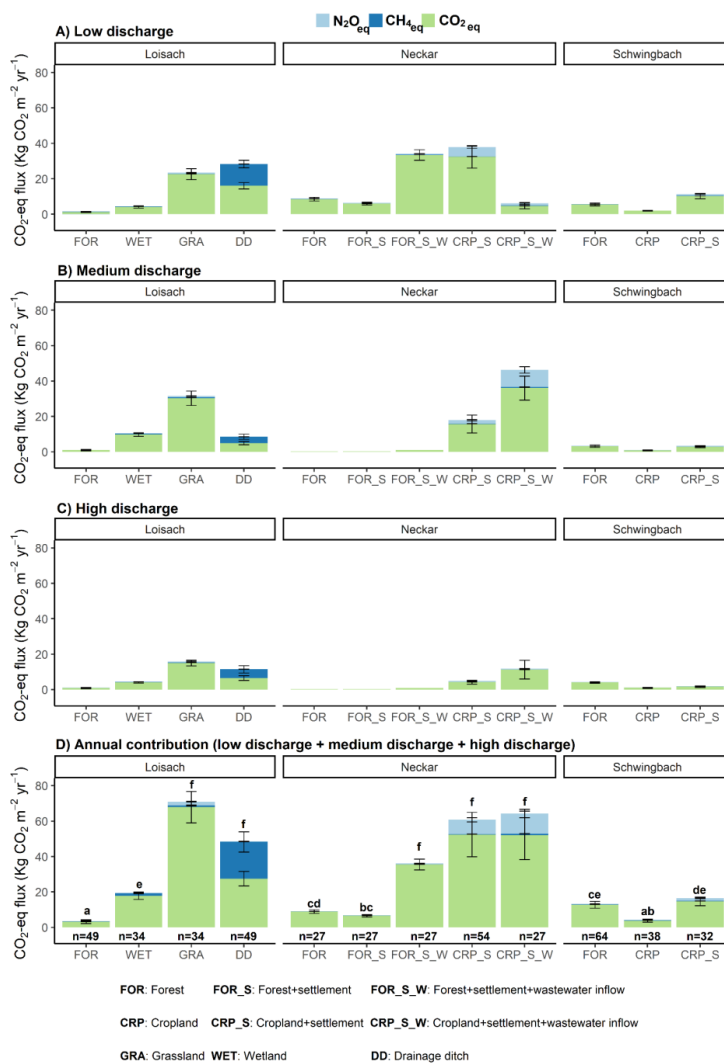
476 annual CO<sub>2</sub>-equivalent emissions from anthropogenic-influenced streams were up to 20 times higher than from  
477 natural forested and wetland streams (~71 kg CO<sub>2</sub> m<sup>-2</sup> yr<sup>-1</sup> vs. ~3 kg CO<sub>2</sub> m<sup>-2</sup> yr<sup>-1</sup> respectively; Fig. 6). It is also  
478 noteworthy that the total annual GHG emission from oligotrophic forested streams in the Loisach catchment  
479 were significantly lower than other forested catchments in the more human influenced Schwingbach and Neckar  
480 sub-catchments (Fig. 6).

481           Regarding different discharge periods, high and medium discharge periods contributed up to 91 % to  
482 total GHG emissions in anthropogenic-influenced streams, but only 4% in forested streams (Fig. 6). Overall, the  
483 high and medium discharge periods contributed the most to the annual fluxes quantified in lower-order streams  
484 (Strahler 1-2) and ditch sampling points, which were prevalent in the Loisach and Schwingbach sub-catchments  
485 (Fig. 6B, C). The opposite was true for larger forested and cropland streams in the Neckar sub-catchment, where  
486 higher annual flux contributions occurred primarily in the low discharge period (Fig. 6A). However, this pattern  
487 did not hold true for cropland streams with the wastewater inflows in the same catchment, with the sites showing  
488 an 82% increase in annual emissions during the high and medium discharge periods (Fig. 6 B, C).

489



24



490

491 Fig. 6: Areal CO<sub>2</sub>-equivalent fluxes (mean ±SE) grouped by GHG type for each land use class during A) low, B)  
 492 medium, and C) high discharge periods. D) represents the total annual fluxes by summing up contributions from  
 493 the three discharge periods. Letters on the bar graphs represent significant differences (p<0.05) in the annual  
 494 areal emissions amongst the land use classes across the three catchments based on Tukey post-hoc analyses from  
 495 the linear mixed-effects models' results (Table 2)





496 **4 Discussion**

497 **4.1 Seasonal variability in GHG concentrations and fluxes**

498 The GHG fluxes quantified from headwater streams and ditches in the three catchments in central and  
499 southern Germany add to the growing evidence that both aquatic ecosystems are significant net emitters of  
500 GHGs to the atmosphere. Seasonal trends in *in situ* GHG concentrations and fluxes were mainly linked to  
501 substrate availability (C and N), discharge and temperature, similar to previous studies on other streams in  
502 temperate climates (Dismore et al., 2013; Herreid et al., 2021). However, the observed seasonality of GHG  
503 fluxes from streams and ditches in our study was further impacted by land use across the three investigated  
504 catchments, with sub-catchments dominated by wetlands or forested land uses exhibiting lower seasonal  
505 variabilities than sub-catchments dominated by agricultural land use or affected by wastewater inflow (Fig. 3).

506 The low *in situ* CO<sub>2</sub> concentrations (< 100% saturation) during summer (Table B2) suggested elevated  
507 photosynthetic uptake within the streams and ditches, which is in line with the results of a recent meta-analysis  
508 on lotic ecosystems (Gómez-Gener et al., 2021). The decline in CO<sub>2</sub> concentrations in summer was most obvious  
509 at the non-forested stream sampling points, with higher canopy cover in the forested areas likely limiting *in situ*  
510 stream photosynthesis due to shading effects. We also found that stream ditch waters were oversaturated with  
511 CO<sub>2</sub> in autumn and winter. These seasons are characterized on the one hand by low discharge and low stream  
512 velocity, conditions which likely reduce degassing rates, and on the other hand by elevated *in situ* C metabolism,  
513 as supported by low DO concentration in autumn, which indicates respiratory O<sub>2</sub> consumption (e.g., Borges et  
514 al., 2018). We attribute the lack of seasonality in CO<sub>2</sub> fluxes (Table B2) to the compensatory effects of  
515 seasonally varying stream velocities and CO<sub>2</sub> source strengths. For example, high CO<sub>2</sub> concentrations and low  
516 gas transfer velocities in autumn and vice versa conditions in spring, resulted in comparable CO<sub>2</sub> fluxes amongst  
517 the two season (Table B2).

518 N<sub>2</sub>O concentrations also varied significantly across seasons, but the pattern differed from that of CO<sub>2</sub>. In  
519 autumn, forested lower-order streams in the Loisach and Schwingbach catchments mainly showed N<sub>2</sub>O  
520 concentrations below atmospheric background concentrations and were temporary sinks of N<sub>2</sub>O (Fig. 3). This  
521 finding could be related to increased inputs of organic matter in these headwater catchments due to leaf fall,  
522 providing additional organic carbon for microbial metabolism in this period, which likely increased the demand  
523 for terminal electron acceptors such as O<sub>2</sub>, NO<sub>3</sub>, as well as N<sub>2</sub>O. This conclusion is also supported by lowest DO  
524 and NO<sub>3</sub>-N concentrations during autumn, which could suggest the dominance of complete denitrification in the  
525 streams (Quick et al., 2019). With decreasing temperatures towards winter, lower productivity and N demand  
526 within the streams resulted in the accumulation of NO<sub>3</sub>-N, which seemed to favor internal N<sub>2</sub>O production as  
527 seen by the positive relationship between the two variables (Fig. 5C). The high sensitivity of the N<sub>2</sub>O reductase  
528 to low temperatures might have further supported elevated N<sub>2</sub>O concentration and fluxes during winter (e.g.,  
529 Holtan-Hartwig et al., 2002). A similar finding of high winter N<sub>2</sub>O concentrations and fluxes was also found in  
530 other temperate streams, alluding to similar controls of temperature and nutrient availability (Herreid et al.,  
531 2021; Galantini et al., 2021). Thus, based on our results, winter periods can significantly contribute to annual  
532 N<sub>2</sub>O emission budgets. Yet, to the best of our knowledge, temperate studies covering the winter period are still  
533 scarce.



26

534 In contrast to CO<sub>2</sub> and N<sub>2</sub>O, neither CH<sub>4</sub> concentrations nor fluxes showed any seasonal trends. Such a  
535 finding is similar to what was found in a global meta-analysis (Stanley et al., 2016), where multiple controls  
536 related to substrate availability, geomorphology and hydrology were shown to result in high spatial-temporal  
537 variance of CH<sub>4</sub>, thus masking any seasonal emission patterns.

#### 538 **4.2 Effect of human impacts on GHG concentrations and fluxes**

539 Anthropogenic-influenced streams and ditches draining predominantly agricultural and settlement areas  
540 showed higher CO<sub>2</sub>-equivalent GHG emissions than forested streams (Fig. 6). Such a finding is similar to other  
541 studies in the temperate region (e.g., Borges et al., 2018; Galantini et al., 2021). The high GHG emissions of  
542 streams and ditches in agricultural and settlement areas is likely due to elevated hydrological inflow (e.g., via  
543 groundwater and interflow) of nitrogen and labile carbon (Lambert et al., 2017, Mwanake et al., 2019) or  
544 terrestrially originating dissolved GHGs linked to lower vegetation cover compared to forested catchments (e.g.,  
545 Mwanake et al., 2022). This interpretation could be supported by the significant positive relationships that we  
546 found between percentage agriculture and stream CO<sub>2</sub>, CH<sub>4</sub> and N<sub>2</sub>O, as well as nitrate concentration, and a  
547 positive trend for DOC (Figure 5).

548 Low DOC:DON ratios have been previously linked to more labile and less aromatic forms of dissolved  
549 organic matter (DOM) (Sebestyen et al., 2008, O'Donnell et al., 2010). We found significantly lower DOC:DON  
550 ratios in streams and ditches in agricultural and settlement areas than in forested streams, suggesting that the  
551 more bioavailable DOM in the human-influenced ecosystems, favored elevated GHGs production through  
552 heterotrophic processes (e.g., Bodmer et al., 2016). Such differences in DOC:DON ratios were also found  
553 amongst forested streams, with a decreasing trend from Loisach, Neckar to Schwingbach catchments, which may  
554 also explain the differences in their GHG emissions (Fig. 6). The differences in the DOM bioavailability of  
555 forested streams in the three catchments may suggest differences in DOM flowpaths during terrestrial-  
556 groundwater-stream interactions. We contend that the moderately sloping streams of the Neckar and  
557 Schwingbach catchments, likely had lower DOC:DON ratios due to longer water residence time and higher  
558 contributions of groundwater inflow (e.g., Sebestyen et al., 2008) than those in the steeper forested catchments  
559 of the Loisach (Table B3). Distinct difference in water stable isotope signatures, i.e. the shift of precipitation vs.  
560 stream water seasonality across the three catchments (data not shown), further supported the difference in water  
561 residence times and their relationships with stream slope (e.g., Zhou et al., 2021).

562 In addition to land use influences, wastewater inflows into streams in agricultural and settlement areas  
563 further increased GHG concentrations and fluxes. The two sampled wastewater effluents, which drained into the  
564 Steinlach and Ammer streams of the Neckar sub-catchments, showed higher GHG concentrations than the  
565 stream water upstream of the inflows (Fig. A5, Table B1), which mainly lead to increased GHG concentration  
566 and fluxes also downstream of the wastewater inflows. This finding is similar to what was found in other  
567 temperate studies comparing stream GHG concentration upstream and downstream of wastewater inflows (e.g.,  
568 Marescaux et al., 2018; Aho et al., 2022). However, due to higher background GHG fluxes in the cropland than  
569 the forested sub-catchments (Fig. 4), differences in the total GHG emissions before and after wastewater inflow  
570 were more pronounced in the forested sub-catchments (Fig. 6). In addition to the pronounced differences in the  
571 quality of the wastewater effluent (Table B1), this finding also shows the importance of background GHG fluxes  
572 as influenced by catchment land use in assessing how wastewater inflows affect riverine GHG emissions.



573            Apart from land use influences, GHG fluxes from streams have been previously shown to decrease  
574 with stream order, as dissolved GHG inputs from groundwater and terrestrial sources also decrease (e.g.,  
575 Hotchkiss et al., 2015, Turner et al., 2015, Mwanake et al., 2022). While our study design was not meant to  
576 explicitly assess stream order influences due to limited replication across a wide range of stream orders, we did  
577 find an opposite trend with stream order. For example, higher-order streams (stream orders > 5) in the Neckar  
578 sub-catchments dominated by croplands and with wastewater influences had mostly higher GHG fluxes than  
579 lower-order streams (stream orders < 3) in the Loisach and Schwingbach catchments. We therefore show a  
580 potential breakdown of stream order-GHG relationships in highly human-impacted lotic ecosystems, with  
581 disproportionately higher GHG emissions than in more natural ecosystems. We also show that significant  
582 nutrient and labile carbon supplies to higher-order streams, which create ideal conditions for GHG production  
583 and emission, may outweigh the physical disadvantages (e.g. lower surface area to volume ratio) of higher-order  
584 streams relative to lower-order streams.

585            Drainage ditches, characterized by low flow velocities and high DOC:DIN ratios, functioned as strong  
586 sources of CO<sub>2</sub> and CH<sub>4</sub> fluxes compared to streams. We assume that the low DO, high DOC, and low NO<sub>3</sub>-N  
587 concentrations, along with high water retention times, supported high *in situ* CH<sub>4</sub> production rates in sediments,  
588 resulting in the overall highest contribution of CH<sub>4</sub> fluxes to total annual GHG emission budgets than  
589 streams (Figure 6). This interpretation is further supported by a significant negative relationship between CH<sub>4</sub> and  
590 DO, as well as NO<sub>3</sub>-N concentrations, and a positive relationship with DOC concentrations, associations which  
591 have also been previously linked to *in situ* methane production in fluvial ecosystems (e.g., Baulch et al., 2011b;  
592 Schade et al., 2016). High CH<sub>4</sub> fluxes from drainage ditches were also found in other studies from both forested  
593 and wetland areas (e.g., Schrier-Uijl et al., 2011; Peacock et al., 2021b). Contrastingly, ditches were only weak  
594 sources or even sinks for atmospheric N<sub>2</sub>O. This finding suggests N<sub>2</sub>O reduction to N<sub>2</sub> via complete  
595 denitrification, an interpretation already made in previous studies on lotic ecosystems (e.g., Baulch et al., 2011;  
596 Mwanake et al., 2019).

#### 597 **4.3 Comparison of GHG flux magnitudes with other regional studies**

598            This study reported among the highest fluvial CO<sub>2</sub> emissions compared to other studies, with significant  
599 mean fluxes of up to 51 g-C m<sup>-2</sup> d<sup>-1</sup> (Table 4). We attribute this finding to moderate-steep slopes such as those  
600 quantified in the mountainous streams of the Loisach catchment or diffuse and point terrestrial dissolved GHG  
601 inputs from the more human-influenced Schwingbach and Neckar catchments, translating to higher fluvial GHG  
602 fluxes (Fig. 6). However, our high CO<sub>2</sub> fluxes are comparable with those quantified from other temperate  
603 streams in Canada and Switzerland with similar moderate-steep slopes and considerable dissolved CO<sub>2</sub> inputs  
604 from terrestrial landscapes (e.g., McDowell & Johnson, 2018; Horgby et al., 2019). The CH<sub>4</sub> fluxes from streams  
605 in this study are comparable with those previously found in temperate sub-catchments with similar land uses and  
606 altitudes, but are lower than those reported from permafrost streams in China (Zhang et al., 2020). Our N<sub>2</sub>O  
607 fluxes from cropland, settlement, and wastewater-influenced streams, are higher than those previously reported  
608 in a mixed landuse catchment (Schade et al., 2016), but our forest N<sub>2</sub>O fluxes are in the same range as those of  
609 other temperate forested streams (Aho et al., 2022). That said, these comparisons may be hampered, particularly  
610 for fluvial N<sub>2</sub>O fluxes, by the limited number of studies currently available (Table 4).



28

611           The average ditch CH<sub>4</sub> fluxes in this study are higher than those reported for forest and wetland draining  
612 ditches in boreal and temperate regions (Table 4: Schrier-Uijl et al., 2011, Peacock et al., 2021b) and the global  
613 mean provided by Peacock et al., (2021), which includes estimates from large canals. In contrast, N<sub>2</sub>O fluxes  
614 from ditches in this study are lower than those quantified from NO<sub>3</sub>-N-rich agricultural ditches in tropical and  
615 temperate regions (Table 4: Harrison & Matson, 2002; Reay et al., 2003).



Table 4: Compilation of GHG emissions from temperate streams and ditches with comparable land use, climate, and altitude ranges.

Land use/ land cover	Climate	Country	Geographical coordinates, Altitude (m)	Number of study reaches	Duration of study	CO <sub>2</sub> -C flux (g m <sup>-2</sup> d <sup>-1</sup> )		CH <sub>4</sub> -C flux (ng m <sup>-2</sup> d <sup>-1</sup> )		N <sub>2</sub> O-N flux (ng m <sup>-2</sup> d <sup>-1</sup> )		Reference
						Range	Mean	Range	Mean	Range	Mean	
Forest/Loisach streams	Temperate	Germany	Table 1 616–2963	3	51	-0.05 – 17.4	2.4	-0.4 – 164	10.5	-9.2 – 20.3	1.1	This study
Forest/Schwülbach streams	Temperate	Germany	Table 1 176–480	5	27	0.08 – 33.4	9.5	-0.02 – 54.6	9.9	-1.6 – 96.6	2.1	This study
Forest/Neckar rivers	Temperate	Germany	Table 1 319–610	1	80	0.6 – 14.7	6.6	0.6 – 28.9	9.1	-6.9 – 5.9	0.3	This study
Forest-settlement/Neckar rivers	Temperate	Germany	Table 1 319–610	1	27	0.6 – 14.9	4.9	0.4 – 17.3	3.9	-7.7 – 6.0	2.2	This study
Forest-settlement+wastewater/Neckar rivers	Temperate	Germany	Table 1 319–610	1	27	1.2 – 71.7	28.3	1.4 – 15.2	6.5	-2.8 – 17.1	3.9	This study
Wetland/Loisach streams	Temperate	Germany	Table 1 616–2963	2	34	2.8 – 25.2	13.3	17.2 – 237.5	101.7	-1.6 – 2.9	0.8	This study
Grassland/Loisach streams	Temperate	Germany	Table 1 616–2963	2	34	6.1 – 115.9	50.7	1.3 – 324.5	73.2	-0.8 – 25.5	12.4	This study
Cropland/Schwülbach streams	Temperate	Germany	Table 1 176–480	3	48	0.3 – 9.0	2.1	0.07 – 5.6	0.9	-0.8 – 18	1.9	This study
Cropland-settlement/Schwülbach streams	Temperate	Germany	Table 1 176–480	2	32	0.6 – 32.0	8.6	0.6 – 52.6	14.9	-0.8 – 22.4	6.5	This study
Cropland-settlement/Neckar rivers	Temperate	Germany	Table 1 319–610	2	54	4.5 – 181.3	39.1	1.6 – 77.5	21	8.4 – 165.7	46.9	This study
Cropland-settlement+wastewater/Neckar rivers	Temperate	Germany	Table 1 319–610	1	27	1.1 – 129.9	38.8	0.8 – 301.9	58.2	6.3 – 198.2	67.6	This study
Forest streams	Temperate	USA	43.0760° N, 107.2903° W	1211–3311	1	253	1.5–6.79	1.3	14.4–576	28.8		Kuhn et al., 2017
Forest streams	Temperate	USA	40.2140° N, 105.4532° W	2780–3505	2	11	0.2–1.6	0.49	0.3–7.8	2.1		Crawford et al., 2015
Forest streams	Temperate	USA	41.6032° N, 73.0877° W	270–810	7	608						Aho et al., 2022
Forest streams	Temperate	USA	41.6032° N, 73.0877° W	270–810	7	608	-1.2 – 152	3.4	0.3 – 2870	28.7		Aho et al., 2021
Forest streams	Temperate	Canada	49.270° N, 122.560° W	1200–3050	1		8.7 – 1980	55.9				McDowell and Johnson, 2018
Mixed streams	Temperate	USA	43.023° N, 71.1219° W	165–348	3	37			6–43.8			Schulte et al., 2016
Mixed streams	Temperate	Switzerland	46.1512° N, 7.0654° E	1190–3051	1	300	13.3 – 494.5	31				Hogby et al., 2019
Mixed streams	Temperate	Europe		34	107	-0.8 – 5.8						Altenmeyer et al., 2021
Grassland drainage ditches	Temperate	Netherlands	Table 1 52.2200° N, 4.5300° E	1–10	7	2 – 63.3	13.7	116.6 – 7933	1532	-0.8 – 7.1	1.2	This study
Wetland drainage ditches	Temperate	Scotland	65.5000° N, 3.2400° W	58–68	10		0.8		606.6			Schrier-Uijl et al., 2011
Agricultural drainage ditches	Temperate				22					1.5 – 15.3	2.5	Reyn et al. 2003



617           **Conclusions**

618           Compared to forests and wetlands, streams and ditches in agricultural and settlement areas were  
619 characterized by significantly higher GHG fluxes with greater intra-annual variabilities. A combination of  
620 wastewater inflows and agricultural land use resulted in the highest riverine CO<sub>2</sub> and N<sub>2</sub>O fluxes, particularly  
621 during high discharge periods with substantial contributions of external dissolved GHGs. In general,  
622 anthropogenic activities resulted in a potential breakdown of the expected decrease of the GHG source strengths  
623 with increasing stream order, as higher-order streams in the Neckar sub-catchments with cropland and settlement  
624 influences had higher concentrations and areal fluxes than small streams in the Loisach and Schwingbach  
625 catchments. As most studies use stream order to upscale local and regional riverine fluxes, we show from our  
626 results that caution must be taken in applying the methodology, particularly across catchments differing in land  
627 use intensity.

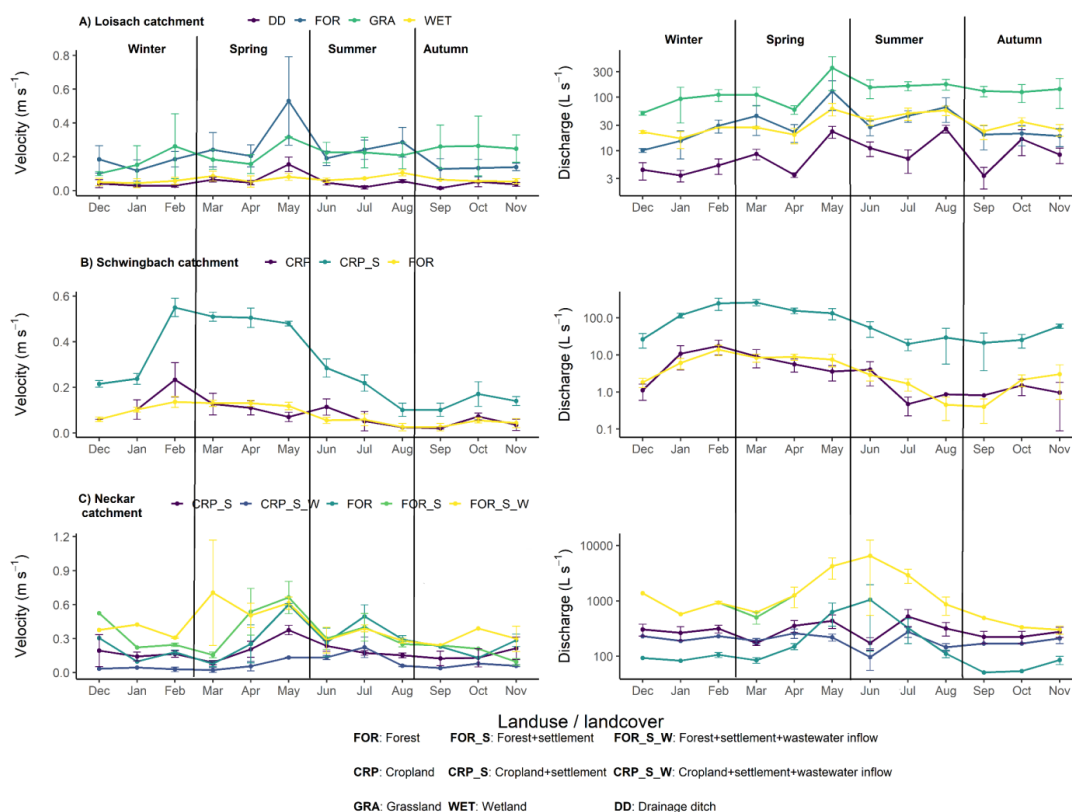
628           In general, our findings indicate that future work should focus more on human-influenced headwater  
629 stream ecosystems, as they contribute disproportionately large annual fluxes and are more temporally variable  
630 than natural ones. Our study also found higher winter N<sub>2</sub>O fluxes, emphasizing the need for continuous sampling  
631 regimes covering full years in order to reduce uncertainty in annual GHG emission estimates. Combining  
632 continuous sampling regimes of all three biogenic GHGs (CO<sub>2</sub>, N<sub>2</sub>O, and CH<sub>4</sub>) across catchments with  
633 contrasting land uses will further constrict riverine emissions and aid in developing targeted emission reduction  
634 mitigation strategies.



31

635 **Appendices**

636 **Appendix A: Figures**



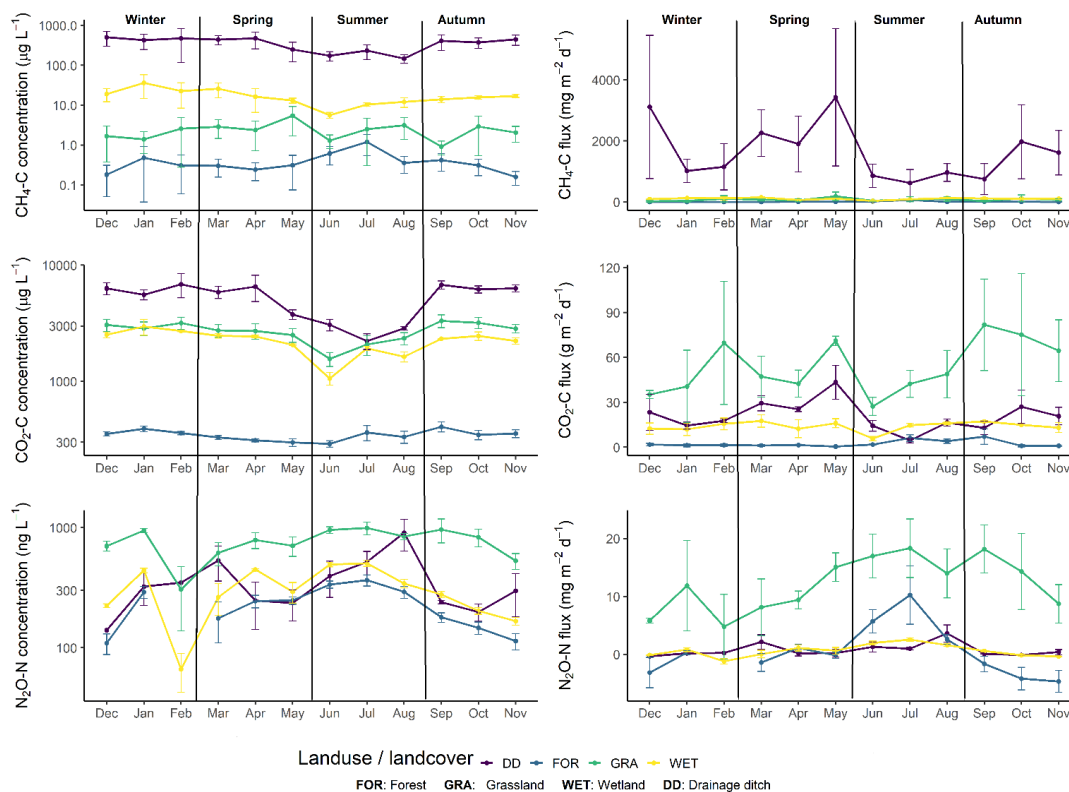
637

638 Fig. A1: Monthly mean  $\pm$  SE velocity and discharge grouped by landuse / landcover classes in the A) Loisach,

639 B) Schwingbach and C) Neckar catchments.



32



640

641

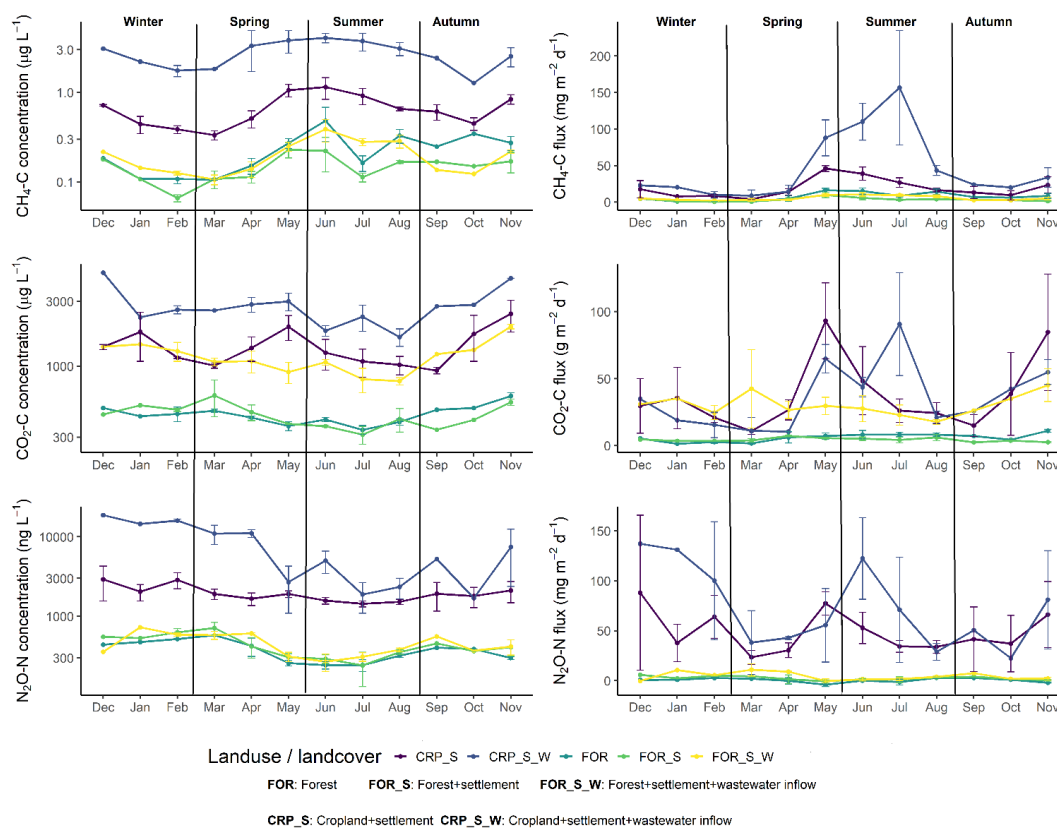
642 Fig. A2: Monthly mean  $\pm$  SE CO<sub>2</sub>, CH<sub>4</sub> and N<sub>2</sub>O concentrations and fluxes at forested (FOR), wetland (WET),

643 grassland (GRA) and ditch (DD) sites in the **Loisach** catchment (see Table 1 methods).





33



644

645

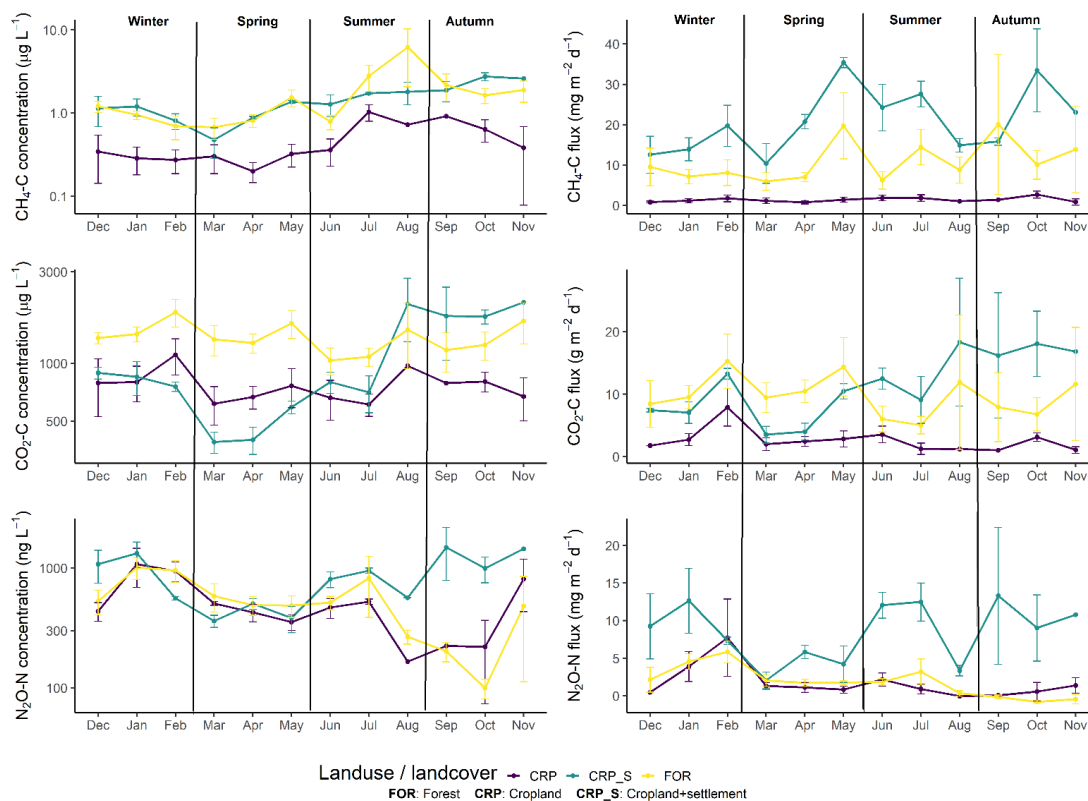
646 Fig. A3: Monthly mean ± SE CO<sub>2</sub>, CH<sub>4</sub> and N<sub>2</sub>O concentrations and fluxes at forested (FOR), forested + urban

647 (FOR\_S), forested + urban + wastewater (FOR\_S\_W), cropland + urban (CRP\_S) and cropland + urban +

648 wastewater (CRP\_S\_W) sites in the Neckar catchment (see Table 1 methods).



34



649

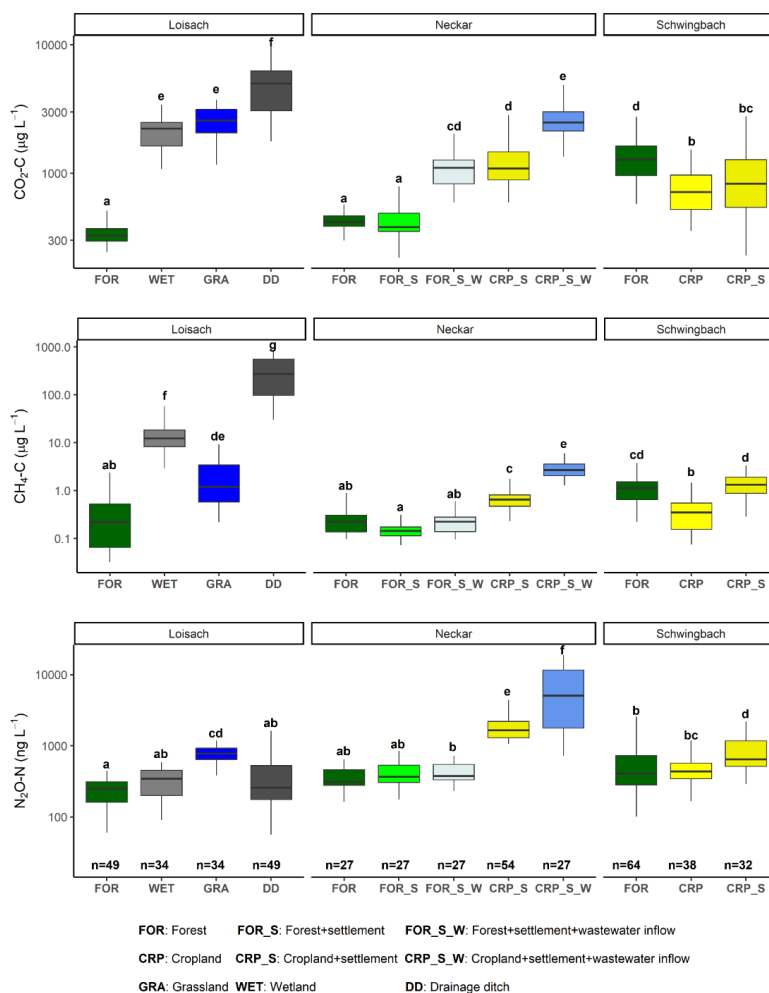
650

651 Fig. A4: Monthly mean  $\pm$  SE CO<sub>2</sub>, CH<sub>4</sub> and N<sub>2</sub>O concentrations and fluxes at forested (FOR), cropland (CRP)

652 and cropland + urban (CRP\_S) sites in the **Schwingbach** catchment (see Table 1 methods).



35



653

654 Fig. A5: Boxplots of CO<sub>2</sub>, CH<sub>4</sub>, and N<sub>2</sub>O concentrations in stream and ditch waters in the three catchments  
 655 grouped by dominating land uses (see Table 1 methods). Letters on top of the boxplots represent significant  
 656 differences (p<0.05) amongst the land use classes across the three catchments based on Tukey post-hoc analyses  
 657 from the linear mixed-effects models' results (Table 3).

658

659

660

661



36

662 **Appendix B: Tables**

663 Table B1: Annual means (+SE) of water chemistry variables and gas concentration measured in the effluents of  
664 the Ammer (WWA) and Steinlach (WWS) wastewater treatment plants.

Water quality variables and discharge	Wastewater effluent quality from inflow zones (Annual Mean $\pm$ SE)	
	Ammer WWA	Steinlach WWS
Temperature ( $^{\circ}$ C)	13.85 $\pm$ 0.61	13.72 $\pm$ 0.65
pH	7.58 $\pm$ 0.07	7.37 $\pm$ 0.09
DO ( $\text{mg L}^{-1}$ )	6.01 $\pm$ 0.32	5.99 $\pm$ 0.34
Specific Conductivity	1017.96 $\pm$ 63.08	776.68 $\pm$ 63.48
NO <sub>3</sub> -N ( $\text{mg L}^{-1}$ )	7.57 $\pm$ 0.6	6.33 $\pm$ 0.47
NH <sub>4</sub> -N ( $\text{mg L}^{-1}$ )	0.14 $\pm$ 0.02	0.09 $\pm$ 0.03
DOC ( $\text{mg L}^{-1}$ )	6.8 $\pm$ 0.33	5.66 $\pm$ 0.58
TDN ( $\text{mg L}^{-1}$ )	8.43 $\pm$ 0.88	7.58 $\pm$ 0.88
CO <sub>2</sub> -C concentration ( $\mu\text{g L}^{-1}$ )	4020.08 $\pm$ 192.75	4529.3 $\pm$ 224.37
CH <sub>4</sub> -C concentration ( $\mu\text{g L}^{-1}$ )	2.13 $\pm$ 0.3	0.73 $\pm$ 0.09
N <sub>2</sub> O-N concentration ( $\text{ng L}^{-1}$ )	9255.11 $\pm$ 1563.23	483.23 $\pm$ 61.35

665

666

667

668

669

670

671

672

673

674

675

676

677



37

678 Table B2: Seasonal means (+SE) of water physico-chemical variables, gas concentration and flux measured in  
 679 the Loisach, Neckar and Schwingbach catchments. Letters beside the means represent significant differences  
 680 ( $p < 0.05$ ) amongst the seasons across the three catchments based on Tukey post-hoc analyses from the linear  
 681 mixed-effects models' results (Table 2).

	Summer	Autumn	Winter	Spring
Temperature ( $^{\circ}\text{C}$ )	14.04 $\pm$ 0.2 <b>d</b>	9.83 $\pm$ 0.32 <b>c</b>	5.55 $\pm$ 0.21 <b>a</b>	8.38 $\pm$ 0.22 <b>b</b>
pH	7.85 $\pm$ 0.03 <b>a</b>	7.88 $\pm$ 0.04 <b>ab</b>	7.98 $\pm$ 0.04 <b>b</b>	7.96 $\pm$ 0.04 <b>ab</b>
DO ( $\text{mg L}^{-1}$ )	8.71 $\pm$ 0.18 <b>a</b>	8.55 $\pm$ 0.29 <b>a</b>	9.63 $\pm$ 0.27 <b>b</b>	9.85 $\pm$ 0.22 <b>b</b>
Specific Conductivity	612.03 $\pm$ 21.8 <b>a</b>	606.91 $\pm$ 28.44 <b>b</b>	600.86 $\pm$ 32.62 <b>ab</b>	555.63 $\pm$ 24.03 <b>a</b>
NO <sub>3</sub> -N ( $\text{mg L}^{-1}$ )	2.54 $\pm$ 0.22 <b>a</b>	2.14 $\pm$ 0.29 <b>a</b>	2.86 $\pm$ 0.28 <b>b</b>	2.6 $\pm$ 0.22 <b>ab</b>
NH <sub>4</sub> -N ( $\text{mg L}^{-1}$ )	0.11 $\pm$ 0.01 <b>a</b>	0.14 $\pm$ 0.02 <b>a</b>	0.13 $\pm$ 0.02 <b>a</b>	0.1 $\pm$ 0.01 <b>a</b>
TN ( $\text{mg L}^{-1}$ )	2.9 $\pm$ 0.22 <b>a</b>	2.49 $\pm$ 0.3 <b>a</b>	3.01 $\pm$ 0.36 <b>b</b>	3 $\pm$ 0.29 <b>ab</b>
DON ( $\text{mg L}^{-1}$ )	0.5 $\pm$ 0.07 <b>a</b>	0.75 $\pm$ 0.15 <b>a</b>	1.56 $\pm$ 0.26 <b>a</b>	1.3 $\pm$ 0.24 <b>a</b>
DOC ( $\text{mg L}^{-1}$ )	4.37 $\pm$ 0.24 <b>a</b>	4.26 $\pm$ 0.36 <b>a</b>	4.1 $\pm$ 0.31 <b>a</b>	4.66 $\pm$ 0.26 <b>a</b>
DOC:DIN	11.45 $\pm$ 2.9 <b>b</b>	7.21 $\pm$ 1.37 <b>ab</b>	4.14 $\pm$ 0.75 <b>a</b>	7.21 $\pm$ 1.81 <b>b</b>
DOC:DON	103.91 $\pm$ 56.91 <b>a</b>	183.33 $\pm$ 140.18 <b>a</b>	13.19 $\pm$ 2.37 <b>a</b>	28.33 $\pm$ 7.31 <b>a</b>
Stream velocity ( $\text{m s}^{-1}$ )	0.18 $\pm$ 0.01 <b>ab</b>	0.12 $\pm$ 0.01 <b>a</b>	0.16 $\pm$ 0.01 <b>ab</b>	0.24 $\pm$ 0.02 <b>b</b>
Discharge $\text{L s}^{-1}$	526.41 $\pm$ 171.4 <b>ab</b>	86.25 $\pm$ 13.07 <b>a</b>	157.3 $\pm$ 31.58 <b>ab</b>	384.08 $\pm$ 96.29 <b>b</b>
CO <sub>2</sub> concentration ( $\mu\text{g-C L}^{-1}$ )	1198.93 $\pm$ 71.66 <b>a</b>	2222.22 $\pm$ 208.63 <b>c</b>	1869.06 $\pm$ 185.95 <b>c</b>	1666.03 $\pm$ 148.04 <b>b</b>
CH <sub>4</sub> concentration ( $\mu\text{g-C L}^{-1}$ )	20.94 $\pm$ 5.36 <b>a</b>	58.08 $\pm$ 17.8 <b>a</b>	46.98 $\pm$ 18 <b>a</b>	40.94 $\pm$ 13.03 <b>a</b>
N <sub>2</sub> O concentration ( $\text{ng-N L}^{-1}$ )	816.06 $\pm$ 75.58 <b>ab</b>	796.45 $\pm$ 169.08 <b>a</b>	1691.19 $\pm$ 400.62 <b>b</b>	1021.38 $\pm$ 185.45 <b>ab</b>
$k_{600} \text{md}^{-1}$	32.31 $\pm$ 3.09 <b>ab</b>	22.71 $\pm$ 2.8 <b>a</b>	24.54 $\pm$ 3.36 <b>ab</b>	33.92 $\pm$ 3.42 <b>b</b>
CO <sub>2</sub> flux ( $\text{mg-C m}^{-2} \text{d}^{-1}$ )	17008.98 $\pm$ 1876.63 <b>a</b>	22710.21 $\pm$ 3422.95 <b>a</b>	14836.51 $\pm$ 1835.54 <b>a</b>	20592.21 $\pm$ 2563.97 <b>a</b>
CH <sub>4</sub> flux ( $\text{mg-C m}^{-2} \text{d}^{-1}$ )	121.65 $\pm$ 30.93 <b>a</b>	233.99 $\pm$ 84.4 <b>a</b>	157.33 $\pm$ 73.04 <b>a</b>	262.87 $\pm$ 89.31 <b>a</b>
N <sub>2</sub> O flux ( $\text{mg-N m}^{-2} \text{d}^{-1}$ )	13.69 $\pm$ 2.22 <b>b</b>	9.63 $\pm$ 2.86 <b>a</b>	16.12 $\pm$ 4.05 <b>b</b>	10.64 $\pm$ 2.11 <b>ab</b>



Table B3: Annual mean ± standard errors of measured water physico-chemical variables, GHG concentration, and flux for land use classes in the Loisach (FOR: forest, WET: wetland, GRA: grassland, and DD: drainage ditches), the Neckar (FOR, FOR\_S: forest+settlement, FOR\_S\_W: forest+settlement+wastewater inflow, CRP\_S: cropland+settlement, and CRP\_S\_W: cropland+settlement+wastewater inflow, and the Schwingbach catchment (FOR, CRP: cropland and CRP\_S). The number of observations in each land use class is represented by "n" in brackets. Letters beside the means represent significant differences ( $p < 0.05$ ) amongst the land use classes across the three catchments based on Tukey post-hoc analyses from the linear mixed-effects models' results (Table 2).

	Loisach				Neckar				Schwingbach			
	FOR (n=49)	WET (n=34)	GRA (n=34)	DD (n=49)	FOR (n=27)	FOR_S (n=27)	FOR_S_W (n=27)	CRP_S_W (n=27)	FOR (n=64)	CRP (n=38)	CRP_S (n=32)	
Temperature (°C)	8 ± 0.5 a	8.6 ± 0.4 ab	9.5 ± 0.2 bd	9 ± 0.5 bc	10.44 ± 1.01 bd	11.6 ± 1.01 de	12.14 ± 0.85 ef	13.06 ± 0.65 f	9.7 ± 0.5 bc	9.9 ± 0.7 cdef	9.8 ± 0.8 bc	
pH	8.3 ± 0.01 de	7.7 ± 0.01 b	7.6 ± 0.01 b	7.3 ± 0.01 a	8.45 ± 0.05 e	8.44 ± 0.05 e	8.07 ± 0.05 cd	7.72 ± 0.08 b	7.7 ± 0.01 b	8 ± 0.01 c	8 ± 0.1 c	
DO (mg L <sup>-1</sup> )	11 ± 0.1 de	8.3 ± 0.2 c	7.4 ± 0.2 b	4.2 ± 0.3 a	11.49 ± 0.39 de	11.57 ± 0.33 de	10.62 ± 0.31 d	8.3 ± 0.29 bc	8.8 ± 0.1 c	8.9 ± 0.1 c	9 ± 0.1 c	
Specific Conductivity	365.1 ± 8.1 a	436.9 ± 9.4 ab	447.7 ± 2.3 bc	484.9 ± 16.2 bcd	738.51 ± 51.37 g	582.07 ± 13.96 de	700.87 ± 31.16 fg	971.46 ± 41.76 h	389.7 ± 18.8 ab	597.2 ± 13 ef	566.4 ± 20.2 ce	
NO <sub>3</sub> -N (mg L <sup>-1</sup> )	0.8 ± 0.01 cd	0.5 ± 0.01 b	0.8 ± 0.01 cd	0.1 ± 0.01 a	0.57 ± 0.04 bc	2.39 ± 0.13 e	3.73 ± 0.29 ef	7.18 ± 0.38 gh	1.5 ± 0.1 d	4.9 ± 0.4 fg	2.3 ± 0.2 e	
NH <sub>4</sub> <sup>+</sup> -N (mg L <sup>-1</sup> )	0.01 ± 0.001 ab	0.01 ± 0.001 a	0.01 ± 0.001 a	0.3 ± 0.001 d	0.07 ± 0.02 bc	0.11 ± 0.01 cd	0.11 ± 0.02 cd	0.14 ± 0.02 d	0.1 ± 0.01 d	0.1 ± 0.01 d	0.1 ± 0.01 d	
TN (mg L <sup>-1</sup> )	0.7 ± 0.01 b	0.4 ± 0.01 a	0.7 ± 0.01 b	0.9 ± 0.1 b	0.73 ± 0.06 b	2.3 ± 0.11 cd	3.92 ± 0.3 ef	6.57 ± 0.19 gh	2.2 ± 0.2 c	6.1 ± 0.5 fg	3 ± 0.3 de	
DON (mg L <sup>-1</sup> )	0.08 ± 0.02 ab	0.03 ± 0.02 a	0.06 ± 0.03 acd	0.45 ± 0.04 cd	0.3 ± 0.05 d	0.26 ± 0.08 bd	1.02 ± 0.33 de	2.76 ± 0.48 e	0.65 ± 0.11 d	1.45 ± 0.24 ce	0.75 ± 0.1 de	
DOC (mg L <sup>-1</sup> )	2.9 ± 0.3 b	1.8 ± 0.1 a	1.5 ± 0.1 a	9.5 ± 0.7 g	5.9 ± 0.67 fg	4.22 ± 0.35 bc	4.12 ± 0.39 cdf	4.67 ± 0.23 ef	4.8 ± 0.2 ef	3.8 ± 0.1 cde	4.7 ± 0.2 ef	
DOC:DON	4.23 ± 0.46 ef	4.48 ± 0.73 ef	2.06 ± 0.22 d	45.14 ± 8.27 h	13.19 ± 2.32 g	1.84 ± 0.24 cd	1.64 ± 0.23 cd	0.62 ± 0.03 a	5.89 ± 1.1 f	1.25 ± 0.17 bc	2.82 ± 0.3 de	
Stream velocity (m s <sup>-1</sup> )	0.22 ± 0.03 cd	0.07 ± 0.01 b	0.22 ± 0.02 cd	37.84 ± 3.02 fg	60.73 ± 30.87 efg	46.02 ± 16.38 dfg	18.06 ± 10.65 acd	6.65 ± 2.54 ab	37.19 ± 15.88 dff	9.02 ± 2.67 ac	13.13 ± 2.9 bcde	
Discharge Ls <sup>-1</sup>	37.7 ± 7.3 c	34.5 ± 3.2 cd	142.1 ± 20.6 ef	0.05 ± 0.01 a	0.3 ± 0.04 de	0.34 ± 0.04 ce	0.4 ± 0.04 e	0.09 ± 0.02 ab	0.09 ± 0.01 ab	0.1 ± 0.01 ab	0.29 ± 0.03 de	
CO <sub>2</sub> -C concentration (µg L <sup>-1</sup> )	337.9 ± 9.1 a	2075.3 ± 107.8 e	2559.5 ± 123.8 e	4913.5 ± 285.4 f	423.85 ± 14.6 a	426.67 ± 24.18 a	1093.04 ± 71.11 cd	1372.92 ± 104.52 d	1380 ± 65.3 d	748.9 ± 45.1 b	1018.1 ± 117.6 bc	
CH <sub>4</sub> -C concentration (µg L <sup>-1</sup> )	0.4 ± 0.1 ab	16.2 ± 2.2 f	2.4 ± 0.4 de	338 ± 37 g	0.25 ± 0.03 ab	0.15 ± 0.01 a	0.23 ± 0.02 ab	3.01 ± 0.25 e	1.5 ± 0.2 cd	0.4 ± 0.1 b	1.5 ± 0.1 d	
N <sub>2</sub> O-N concentration (µg L <sup>-1</sup> )	240.9 ± 16.3 a	323 ± 25.1 ab	771.1 ± 42.2 cd	431.3 ± 64.9 ab	355.91 ± 24.26 ab	405.94 ± 32.61 ab	421.75 ± 28.5 b	1846.46 ± 106.37 e	569 ± 59.6 b	540 ± 64.5 bc	864.5 ± 89.4 d	
k <sub>100</sub> md <sup>-1</sup>	80.9 ± 10.6 f	10.5 ± 0.7 bc	31.5 ± 3.1 df	6.5 ± 0.6 a	52.58 ± 5.1 f	37.66 ± 3.56 ef	43.41 ± 3.2 ef	19.95 ± 2.54 ef	11.7 ± 1.1 ac	7.1 ± 0.9 ab	22.9 ± 1.8 de	
CO <sub>2</sub> -C flux (g m <sup>-2</sup> d <sup>-1</sup> )	2.39 ± 0.4 a	13.33 ± 0.9 df	50.71 ± 5.3 g	20.52 ± 1.9 ef	6.66 ± 0.8 cd	4.89 ± 0.55 bc	28.26 ± 2.8 fg	39.16 ± 6.3 fg	9.54 ± 0.9 cd	2.8 ± 0.4 ab	10.96 ± 1.3 cde	
CH <sub>4</sub> -C flux (mg m <sup>-2</sup> d <sup>-1</sup> )	10.5 ± 4.3 ab	101.7 ± 8.3 f	73.2 ± 15.7 de	1532.9 ± 244.8 g	9.09 ± 1.5 bc	3.88 ± 0.7 ac	6.54 ± 0.81 bc	21.09 ± 2.37 d	9.9 ± 1.3 c	1.5 ± 0.2 a	21.5 ± 2.2 de	
N <sub>2</sub> O-N flux (mg m <sup>-2</sup> d <sup>-1</sup> )	1.1 ± 0.9 a	0.8 ± 0.2 a	12.4 ± 1.4 c	1.2 ± 0.4 a	0.32 ± 0.03 a	2.2 ± 0.64 a	3.96 ± 0.85 ab	46.92 ± 5.02 d	2.1 ± 0.3 a	1.9 ± 0.6 a	8.8 ± 1.1 bc	



Table B4: Indices highlighting the performance of the best-fit SEMs, which indicate significant interaction pathways of both direct and indirect drivers of in-situ GHG concentrations in temperate streams, rivers, and drainage ditches. The goodness of fit index (GFI), comparative fit index (CFI), Tucker lewis index, standardized root mean square residual (SRMR), and root means squared error of approximation (RMSEA) are measures of model goodness of fit, while the parsimony fit index (PNFI) compares the best-fit model to the theoretical-model.

Greenhouse gas (GHG)	Performance indices for the best-fit SEMs						Model comparison	
	GFI	CFI	TLI	SRMR	RMSEA	r <sup>2</sup>	PNFI	
							Theoretical SEM	Best-fit SEM
CO <sub>2</sub> concentration (µg-C L <sup>-1</sup> )	1.00	1.00	1.00	0.02	<0.01	0.60	0.13	0.22
CH <sub>4</sub> concentration (µg-C L <sup>-1</sup> )	1.00	1.00	1.00	0.02	<0.01	0.66	0.13	0.22
N <sub>2</sub> O concentration (ng-N L <sup>-1</sup> )	0.99	1.00	0.98	0.03	0.04	0.46	0.13	0.22

**Best-fit SEM structure:-**

1. Log GHG = DO + DOC + Log NO<sub>3</sub> + agricultural area + wastewater inflow + stream velocity
2. Log NO<sub>3</sub> = DO + agricultural area + wastewater inflow + stream velocity
3. DOC = agricultural area
4. DO = DOC + stream velocity

**Goodness of fit assesment:-** GFI, CFI and TLI: 0.90 - 0.95; Good fit and >0.95 Excellent fit

SRMR and RMSEA: 0.05 - 0.08; Good fit and <0.05 Excellent fit



40

#### **Data availability**

Our institute is currently constructing an own data infrastructure to host all available data from its scientist and link it to the main KIT database. We are working currently with our institute's data department to provide a publicly accessible DOI link for all our research data as directed by our institute's policy. We hope the data will be soon available before the review process completes. Reviewers are however invited to ask for the data anytime during the review process and it will be provided by the corresponding author via email.

#### **Author contribution**

RM, RK, GG, CG, and KB designed the field experiments. RK, KB, TH, and LB provided the infrastructural funding and RM and EW did the field and laboratory work. RM did the statistical analysis, consulting with RK and GG. RM prepared the first draft manuscript, consulting with RK. All co-authors contributed to the final version.

#### **Acknowledgments**

This research was funded by the German academic exchange service (DAAD) as part of RM's doctoral studies. Infrastructure for the research was provided by the TERENO Bavarian Alps/ Pre-Alps Observatory, funded by the Helmholtz Association and the Federal Ministry of Education and Research (BMBF). The authors would like to thank the entire laboratory staff at Karlsruhe Institute of Technology, Campus Alpin, Justus Liebig University Giessen, and the University of Tübingen for providing logistical support and supporting the gas and nutrient analyses. We also acknowledge the contributions of Alisson Kolar, Paul Levin Degott, Franz Weyerer, and Raphael Boehm during the field campaigns.

#### **Declaration of competing interest**

The authors declare that they have no conflict of interest.





## References

- Aho, K. S., & Raymond, P. A.: Differential response of greenhouse gas evasion to storms in forested and wetland streams. *Journal of Geophysical Research: Biogeosciences* **124**, 649–662. <https://doi.org/10.1029/2018JG004750>, 2019.
- Aho, K. S., Fair, J. H., Hosen, J. D., Kyzivat, E. D., Logozzo, L. A., Rocher-Ros, G., Weber, L. C., Yoon, B., & Raymond, P. A.: Distinct concentration-discharge dynamics in temperate streams and rivers: CO<sub>2</sub> exhibits chemostasis while CH<sub>4</sub> exhibits source limitation due to temperature control. *Limnology and Oceanography*, **66**, 3656–3668. <https://doi.org/10.1002/lno.11906>, 2021.
- Aho, K. S., Fair, J. H., Hosen, J. D., Kyzivat, E. D., Logozzo, L. A., Weber, L. C., Yoon, B., Zarnetske, J. P., & Raymond, P. A.: An intense precipitation event causes a temperate forested drainage network to shift from N<sub>2</sub>O source to sink. *Limnology and Oceanography*, **67**, S242–S257. <https://doi.org/10.1002/lno.12006>, 2022.
- Allen, G. H., Pavelsky, T. M., Barefoot, E. A., Lamb, M. P., Butman, D., Tashie, A., & Gleason, C. J.: Similarity of stream width distributions across headwater systems. *Nature Communications* **9**, 610. <https://doi.org/10.1038/A41467-018-02991-w>, 2018.
- Audet, J., Bastviken, D., Bundschuh, M., Buffam, I., Feckler, A., Klemetsson, L., Laudon, H., Löfgren, S., Natchimuthu, S., Öquist, M., Peacock, M., & Wallin, M. B.: Forest streams are important sources for nitrous oxide emissions. *Global Change Biology* **26**, 629–641. <https://doi.org/10.1111/gcb.14812>, 2019.
- Battin, T. J., Kaplan, L. A., Findlay, S., Hopkinson, C. S., Marti, E., Packman, A. I., Newbold, J. D., & Sabater, F.: Biophysical controls on organic carbon fluxes in fluvial networks. *Nature Geoscience* **1**, 95–100. <https://doi.org/10.1038/ngeo101>, 2008.
- Baulch, H. M., Schiff, S. L., Maranger, R., & Dillon, P. J.: Nitrogen enrichment and the emission of nitrous oxide from streams. *Global Biogeochemical Cycles* **25**. <https://doi.org/10.1029/2011GB004047>, 2011.
- Baulch, H. M., Dillon, P. J., Maranger, R., & Schiff, S. L.: Diffusive and ebullitive transport of methane and nitrous oxide from streams: Are bubble-mediated fluxes important? *Journal of Geophysical Research: Biogeosciences* **116**. <https://doi.org/10.1029/2011JG001656>, 2011a.
- Beaulieu, J. J., Arango, C. P., & Tank, J. L.: The effects of season and agriculture on nitrous oxide production in headwater streams. *Journal of Environment Quality* **38**, 637. <https://doi.org/10.2134/jeq2008.0003>, 2009.
- Bodmer, P., Heinz, M., Pusch, M., Singer, G., & Premke, K.: Carbon dynamics and their link to dissolved organic matter quality across contrasting stream ecosystems. *Science of the Total Environment* **553**, 574–586. <https://doi.org/10.1016/j.scitotenv.2016.02.095>, 2016.
- Bolleter, W. T., Bushman, C. J., & Tidwell, P. W.: Spectrophotometric determination of ammonia as indophenol. *Analytical Chemistry* **33**, 592–594. <https://doi.org/10.1021/ac60172a034>, 1961.
- Borges, A. V., Darchambeau, F., Lambert, T., Bouillon, S., Morana, C., Brouyère, S., Hakoun, V., Jurado, A.,



- Tseng, H.C., Descy, J.P., & Roland, F.A.: Effects of agricultural land use on fluvial carbon dioxide, methane and nitrous oxide concentrations in a large European river, the Meuse (Belgium). *Science of the Total Environment* **610–611**, 342–355. <https://doi.org/10.1016/j.scitotenv.2017.08.047>, 2018.
- Borges, A.V., Darchambeau, F., Lambert, T., Morana, C., Allen, G.H., Tambwe, E., Toengaho Sembaito, A., Mambo, T., Nlandu Wabakhangazi, J., Descy, J.P., & Teodoru, C.R.: Variations in dissolved greenhouse gases (CO<sub>2</sub>, CH<sub>4</sub>, N<sub>2</sub>O) in the Congo river network overwhelmingly driven by fluvial-wetland connectivity. *Biogeosciences* **16**, 3801–3834. <https://doi.org/10.5194/bg-16-3801-2019>, 2019.
- Crawford, J. T., Dornblaser, M. M., Stanley, E. H., Clow, D. W., & Striegl, R. G.: Source limitation of carbon gas emissions in high-elevation mountain streams and lakes. *Journal of Geophysical Research: Biogeosciences*, **120**, 952-964. <https://doi.org/10.1002/2014JG002861>, 2015.
- Dinsmore, K. J., Wallin, M. B., Johnson, M. S., Billett, M. F., Bishop, K., Pumpanen, J., & Ojala, A.: Contrasting CO<sub>2</sub> concentration discharge dynamics in headwater streams: A multi-catchment comparison. *Journal of Geophysical Research: Biogeosciences*, **118**, 445-461. <https://doi.org/10.1002/jgrg.20047>, 2013.
- Drake, T. W., Raymond, P. A., & Spencer, R. G.: Terrestrial carbon inputs to inland waters: A current synthesis of estimates and uncertainty. *Limnology and Oceanography Letters*, *3*(3), 132-142. <https://doi.org/10.1002/lol2.10055>, 2018.
- Galantini, L., Lapierre, J. F., & Maranger, R.: How are greenhouse gases coupled across seasons in a large temperate river with differential land use?. *Ecosystems*, **24**, 2007-2027. <https://doi.org/10.1007/A10021-021-00629-5>, 2021.
- Gomez-Gener, L., Rocher-Ros, G., Battin, T., Cohen, M.J., Dalmagro, H.J., Dinsmore, K.J., Drake, T.W., Duvert, C., Enrich-Prast, A., Horgby, Å., & Johnson, M.S.: Global carbon dioxide efflux from rivers enhanced by high nocturnal emissions. *Nature Geoscience*, **14**, 289-294. <https://doi.org/10.1038/A41561-021-00722-3>, 2021.
- Glaser, C., Schwientek, M., Junginger, T., Gilfedder, B.S., Frei, S., Werneburg, M., Zwiener, C., & Zarfl, C.: Comparison of environmental tracers including organic micropollutants as groundwater exfiltration indicators into a small river of a karstic catchment. *Hydrological Processes*, **34**, 4712-4726. <https://doi.org/10.1002/hyp.13909>, 2020.
- Gore, J. A.: Discharge measurements and streamflow analysis. In F. R. Hauer & G. A. Lamberti (Eds.), *Methods in stream ecology*. (2<sup>nd</sup> ed., chap. 3, pp. 51–77). Cambridge, MA: Academic Press. <https://doi.org/10.1016/B978-012332908-0.50005-X>, 2007.
- Intergovernmental Panel on Climate Change.: Climate change 2013—the physical science basis: Working group I contribution to the fifth assessment report of the Intergovernmental Panel on Climate Change. Cambridge: Cambridge University Press. doi:10.1017/CBO9781107415324, 2014.
- Hall Jr, R. O., & Ulseth, A. J.: Gas exchange in streams and rivers. *Wiley Interdisciplinary Reviews: Water*, *7*(1), e1391. <https://doi.org/10.1002/wat2.1391>, 2020.



- Harrison, J., & Matson, P.: Patterns and controls of nitrous oxide emissions from waters draining a subtropical agricultural valley. *Global Biogeochemical Cycles*, **17**. <https://doi.org/10.1029/2002GB001991>, 2003.
- Herreid, A. M., Wymore, A. S., Varner, R. K., Potter, J. D., & McDowell, W. H.: Divergent controls on stream greenhouse gas concentrations across a land-use gradient. *Ecosystems*, **24**, 1299-1316. <https://doi.org/10.1007/A10021-020-00584-7>, 2021.
- Holtan-Hartwig, L., Dörsch, P., & Bakken, L. R.: Low temperature control of soil denitrifying communities: kinetics of N<sub>2</sub>O production and reduction. *Soil Biology and Biochemistry*, **34**, 1797-1806. [https://doi.org/10.1016/S0038-0717\(02\)00169-4](https://doi.org/10.1016/S0038-0717(02)00169-4), 2002.
- Horgby, Å., Boix Canadell, M., Ulseth, A. J., Vennemann, T. W., & Battin, T. J.: High-resolution spatial sampling identifies groundwater as driver of CO<sub>2</sub> dynamics in an Alpine stream network. *Journal of Geophysical Research: Biogeosciences*, **124**, 1961-1976. <https://doi.org/10.1029/2019JG005047>, 2019.
- Hotchkiss, E. R., Hall Jr, R. O., Sponseller, R. A., Butman, D., Klaminder, J., Laudon, H., Rosvall, M., & Karlsson, J.: Sources of and processes controlling CO<sub>2</sub> emissions change with the size of streams and rivers. *Nature Geoscience* **8**, 696–699. <https://doi.org/10.1038/ngeo2507>, 2015.
- Kuhn, C., Bettigole, C., Glick, H. B., Seegmiller, L., Oliver, C. D., & Raymond, P.: Patterns in stream greenhouse gas dynamics from mountains to plains in northcentral Wyoming. *Journal of Geophysical Research: Biogeosciences*, **122**, 2173-2190. <https://doi.org/10.1002/2017JG003906>, 2017.
- Flury, S., & Ulseth, A. J.: Exploring the sources of unexpected high methane concentrations and fluxes from alpine headwater streams. *Geophysical Research Letters*, **46**, 6614-6625. <https://doi.org/10.1029/2019GL082428>, 2019.
- Lambert, T., Bouillon, S., Darchambeau, F., Morana, C., Roland, F. A. E., Descy, J., & Borges, A. V.: Effects of human land use on the terrestrial and aquatic sources of fluvial organic matter in a temperate river basin (The Meuse River, Belgium). *Biogeochemistry* **136**, 191–211. <https://doi.org/10.1007/A10533-017-0387-9>, 2017.
- Li, M., Peng, C., Zhang, K., Xu, L., Wang, J., Yang, Y., Li, P., Liu, Z., & He, N.: Headwater stream ecosystem: an important source of greenhouse gases to the atmosphere. *Water Research*, **190**, 116738. <https://doi.org/10.1016/j.watres.2020.116738>, 2021.
- Marescaux, A., Thieu, V., & Garnier, J.: Carbon dioxide, methane and nitrous oxide emissions from the human-impacted Seine watershed in France. *Science of the Total Environment*, **643**, 247-259. <https://doi.org/10.1016/j.scitotenv.2018.06.151>, 2018.
- McDowell, M. J., & Johnson, M. S.: Gas transfer velocities evaluated using carbon dioxide as a tracer show high streamflow to be a major driver of total CO<sub>2</sub> evasion flux for a headwater stream. *Journal of Geophysical Research: Biogeosciences*, **123**, 2183-2197. <https://doi.org/10.1029/2018JG004388>, 2018.
- Mwanake, R. M., Gettel, G. M., Aho, K. S., Namwaya, D. W., Masese, F. O., Butterbach-Bahl, K., & Raymond, P. A.: Land use, not stream order, controls N<sub>2</sub>O concentration and flux in the upper Mara River basin, Kenya. *Journal of Geophysical Research: Biogeosciences* **124**, 3491–3506.



<https://doi.org/10.1029/2019jg005063>, 2019.

- Mwanake, R. M., Gettel, G. M., Ishimwe, C., Wangari, E. G., Butterbach-Bahl, K., & Kiese, R.: Basin-scale estimates of greenhouse gas emissions from the Mara River, Kenya: Importance of discharge, stream size, and land use/land cover. *Limnology and Oceanography*, **67**, 1776-1793. <https://doi.org/10.1002/lno.12166>, 2022.
- O'Donnell, J. A., Aiken, G. R., Kane, E. S., & Jones, J. B.: Source water controls on the character and origin of dissolved organic matter in streams of the Yukon River basin, Alaska. *Journal of Geophysical Research: Biogeosciences*, **115**. <https://doi.org/10.1029/2009JG001153>, 2010.
- Patton, C. J., & Kryskalla, J. R.: Colorimetric determination of nitrate plus nitrite in water by enzymatic reduction, automated discrete analyzer methods. *US Geological Survey Techniques and Methods, Book 5* **34**. <https://doi.org/10.3133/tm5B8>, 2011.
- Peacock, M., Audet, J., Bastviken, D., Futter, M.N., Gauci, V., Grinham, A., Harrison, J.A., Kent, M.S., Kosten, S., Lovelock, C.E., & Veraart, A.J.: Global importance of methane emissions from drainage ditches and canals. *Environmental Research Letters*, **16**, 044010. <https://doi.org/10.1088/1748-9326/abeb36>, 2021.
- Peacock, M., Granath, G., Wallin, M. B., Högbom, L., & Futter, M. N.: Significant Emissions From Forest Drainage Ditches—An Unaccounted Term in Anthropogenic Greenhouse Gas Inventories?. *Journal of Geophysical Research: Biogeosciences*, **126**. <https://doi.org/10.1029/2021JG006478>, 2021a.
- Quick, A. M., Reeder, W. J., Farrell, T. B., Tonina, D., Feris, K. P., & Benner, S. G.: Nitrous oxide from streams and rivers: A review of primary biogeochemical pathways and environmental variables. *Earth-science reviews*, **191**, 224-262. <https://doi.org/10.1016/j.earscirev.2019.02.021>, 2019.
- Raymond, P.A., Zappa, C.J., Butman, D., Bott, T.L., Potter, J., Mulholland, P., Laursen, A.E., McDowell, W.H. & Newbold, D.: Scaling the gas transfer velocity and hydraulic geometry in streams and small rivers. *Limnology and Oceanography* **2**, 41–53. <https://doi.org/10.1215/21573689-1597669>, 2012.
- Reay, D. S., Smith, K. A., & Edwards, A. C.: Nitrous oxide emission from agricultural drainage waters. *Global Change Biology*, **9**, 195-203. <https://doi.org/10.1046/j.1365-2486.2003.00584.x>, 2003.
- Rocher-Ros, G., Sponseller, R. A., Lidberg, W., Mörth, C. M., & Giesler, R.: Landscape process domains drive patterns of CO<sub>2</sub> evasion from river networks. *Limnology and Oceanography Letters*, **4**, 87-95. <https://doi.org/10.1002/lol2.10108>, 2019.
- Schade, J. D., Bailio, J., & McDowell, W. H.: Greenhouse gas flux from headwater streams in New Hampshire, USA: Patterns and drivers. *Limnology and Oceanography* **61**, 165–174. <https://doi.org/10.1002/lno.10337>, 2016.
- Schrier-Uijl, A. P., Veraart, A. J., Leffelaar, P. A., Berendse, F., & Veenendaal, E. M.: Release of CO<sub>2</sub> and CH<sub>4</sub> from lakes and drainage ditches in temperate wetlands. *Biogeochemistry*, **102**, 265-279. <https://doi.org/10.1007/A10533-010-9440-7>, 2011.
- Schumacker, R. E., & Lomax, R. G.: A Beginner's Guide to Structural Equation Modeling (4th Ed.). New York: Routledge. 2016.



45

- Sebestyen, S. D., Boyer, E. W., Shanley, J. B., Kendall, C., Doctor, D. H., Aiken, G. R., & Ohte, N.: Sources, transformations, and hydrological processes that control stream nitrate and dissolved organic matter concentrations during snowmelt in an upland forest. *Water Resources Research*, **44**.  
<https://doi.org/10.1029/2008WR006983>, 2008.
- Shelley, F., Grey, J., & Trimmer, M.: Widespread methanotrophic primary production in lowland chalk rivers. *Proceedings of the Royal Society B: Biological Sciences*, **281** (1783).  
<https://doi.org/10.1098/rspb.2013.2854mWAN>, 2014.
- Stanley, E. H., Casson, N. J., Christel, S. T., Crawford, J. T., Loken, L. C., & Oliver, S. K.: The ecology of methane in streams and rivers: patterns, controls, and global significance. *Ecological Monographs* **86**, 146–171. <https://doi.org/10.1890/15-1027>, 2016.
- Strahler, A. N.: Hypsometric (area-altitude) analysis of erosional topography. *GSA Bulletin* **63**, 1117–1142.  
[https://doi.org/10.1130/0016-7606\(1952\)63\[1117:HAAOET\]2.0.CO;2](https://doi.org/10.1130/0016-7606(1952)63[1117:HAAOET]2.0.CO;2), 1952.
- Turner, P. A., Griffis, T. J., Lee, X., Baker, J. M., Venterea, R. T., & Wood, J. D.: Indirect nitrous oxide emissions from streams within the US Corn Belt scale with stream order. *Proceedings of the National Academy of Sciences* **112**, 9839–9843. <https://doi.org/10.1073/pnas.1503598112>, 2015.
- Wallin, M. B., Audet, J., Peacock, M., Sahlée, E., & Winterdahl, M.: Carbon dioxide dynamics in an agricultural headwater stream driven by hydrology and primary production. *Biogeosciences* **17**, 2487–2498.  
<https://doi.org/10.5194/bg-17-2487-2020>, 2020.
- Wallin, M.B., Campeau, A., Audet, J., Bastviken, D., Bishop, K., Kokic, J., Laudon, H., Lundin, E., Löfgren, S., Natchimuthu, S. and Sobek, S.: Carbon dioxide and methane emissions of Swedish low-order streams—A national estimate and lessons learnt from more than a decade of observations. *Limnology and Oceanography* **3**, 156–167. <https://doi.org/10.1002/lo12.10061>, 2018.
- Wang, D.; Ye, W., Wu, G., Li, R., Guan, Y., Zhang, W., Wang, J., Shan, Y., Hubacek, K.: Greenhouse gas emissions from municipal wastewater treatment facilities in China from 2006 to 2019. *Sci Data* **9**, 317.  
<https://doi.org/10.1038/s41597-022-01439-7>, 2022.
- Wangari, E.G., Mwanake, R.M., Kraus, D., Werner, C., Gettel, G.M., Kiese, R., Breuer, L., Butterbach-Bahl, K. and Houska, T.: Number of chamber measurement locations for accurate quantification of landscape-scale greenhouse gas fluxes: Importance of land use, seasonality, and greenhouse gas type. *Journal of Geophysical Research: Biogeosciences*, **127**. <https://doi.org/10.1029/2022JG006901>, 2022.
- Winkler, K., Fuchs, R., Rounsevell, M., & Herold, M.: Global land use changes are four times greater than previously estimated. *Nature communications*, **12**, 1–10. <https://doi.org/10.1038/A41467-021-22702-2>, 2021.
- Zhang, L., Xia, X., Liu, S., Zhang, S., Li, S., Wang, J., Wang, G., Gao, H., Zhang, Z., Wang, Q. and Wen, W.: Significant methane ebullition from alpine permafrost rivers on the East Qinghai–Tibet Plateau. *Nature Geoscience*, **13**, 349–354. <https://doi.org/10.1038/A41561-020-0571-8>, 2020.
- Zhang, W., Li, H., Xiao, Q., & Li, X.: Urban rivers are hotspots of riverine greenhouse gas (N<sub>2</sub>O, CH<sub>4</sub>, CO<sub>2</sub>)



emissions in the mixed-landscape chaohu lake basin. *Water Research*, **189**, 116624.

<https://doi.org/10.1016/j.watres.2020.116624>, 2021.

Zhou, J., Liu, G., Meng, Y., Xia, C., Chen, K., & Chen, Y.: Using stable isotopes as tracer to investigate hydrological condition and estimate water residence time in a plain region, Chengdu, China. *Scientific reports*, **11**, 1-12. <https://doi.org/10.1038/s41598-021-82349-3>, 2021.